

Evaluating the S-isotope fractionation associated with Phanerozoic pyrite burial

Nanping Wu^a, James Farquhar^{a,c,*}, Harald Strauss^b, Sang-Tae Kim^a,
Donald E. Canfield^c

^a Department of Geology, University of Maryland, College Park, MD 20740, USA

^b Institut für Geologie und Paläontologie, Westfälische Wilhelms-Universität Münster, Germany

^c NORDCEE, and Institute of Biology, Syddansk Universitet, 5020 Odense C, Denmark

Received 2 February 2009; accepted in revised form 8 December 2009; available online 24 December 2009

Abstract

This study examines the sulfur isotope record of seawater sulfate proxies using $\delta^{34}\text{S}$ and $\Delta^{33}\text{S}$ to place constraints on the average global fractionation ($\Delta^{34}\text{S}_{\text{py}}$) associated with pyrite formation and burial and the exponent λ that relates variations of the $^{34}\text{S}/^{32}\text{S}$ to variations of the $^{33}\text{S}/^{32}\text{S}$. The results presented here use an analysis of the sulfur isotope record from seawater sulfate proxies and sedimentary sulfide to extract this quantity as the arithmetic difference between $\delta^{34}\text{S}$ of seawater sulfate and contemporaneous sulfide. It also uses an independent method that draws on inferences about the $\Delta^{33}\text{S}$ evolution of seawater sulfate to evaluate this further. These two methods yield similar results suggesting that $\Delta^{34}\text{S}_{\text{py}}$ and λ changed over the course of the Phanerozoic from slightly lower values of $\Delta^{34}\text{S}_{\text{py}}$ (lower values of λ) in the early Phanerozoic (Cambrian–Permian) to higher values of $\Delta^{34}\text{S}_{\text{py}}$ (higher values of λ) starting in the Triassic. This change of $\Delta^{34}\text{S}_{\text{py}}$ and the exponent λ is interpreted to reflect a change in the proportion of sulfide that was reoxidized and processed by bacterial disproportionation on a global scale. The revised record of $\Delta^{34}\text{S}_{\text{py}}$ also yields model pyrite burial curves making them more closely resemble model evolution curves for other element systems and global sea level curves. It is suggested that possible links to sea level may occur via changes in the area of submerged continental shelves which would provide additional loci for pyrite burial.

The slightly different constraints used by the two approaches to calculate this fractionation may allow for additional information to be obtained about the sulfur cycle with future studies. For instance, the correspondence of these results suggests that the inferred variation of $^{34}\text{S}/^{32}\text{S}$ of pyrite is real, and that there is no significant missing sink of fractionated sulfur at the resolution of the present study (such as might be associated with organic sulfur). Burial of organic sulfur may, however, have been important at some times in the Phanerozoic and shorter timescale deviations between results provided by these methods may be observed with higher resolution sampling. If observed, this would suggest either that the record for pyrite (or less likely sulfate) is biased, or that another sink (possibly as organic sulfur) was important during these times in the Phanerozoic.

© 2009 Elsevier Ltd. All rights reserved.

1. INTRODUCTION AND CONTEXT

Sulfur has four stable isotopes (^{32}S , ^{33}S , ^{34}S , and ^{36}S) with natural abundances of approximately 95.04%, 0.75%, 4.20%, and 0.01%, respectively (Coplen et al., 2002). Among these there are three, independent isotope ratios that can be determined and used for geological interpretation. In the context of the global sulfur cycle, variations

* Corresponding author. Address: Department of Geology, University of Maryland, College Park, MD 20740, USA.
E-mail address: jfarquha@geol.umd.edu (J. Farquhar).

in these ratios are considered to reflect links with other element cycles, climate, and tectonics. For instance, recent studies by Kurtz et al. (2003) have used models to explore the coupling between the carbon and sulfur cycles, examining short timescale (~ 1 My) variations in the $\delta^{34}\text{S}^1$ of marine barite, and classic studies have used models to explore the controls on $\delta^{34}\text{S}$ of the marine pools and their links to weathering, pyrite burial, and sea level/tectonics on longer timescales (e.g., Claypool et al., 1980; Berner and Raiswell, 1983; Garrels and Lerman, 1984; Holser et al., 1988).

Dissolved sulfate in the oceans has been a recurring focus of these studies because it is one of the few large, well-mixed sulfur reservoirs on Earth, because it can be studied with the use of proxies such as marine barite, carbonate associated sulfate, and evaporites (Bottrell and Newton, 2006), and because fluctuations of its isotopic composition with time record variations in the proportion of seawater sulfate lost to pyrite burial (Claypool et al., 1980; Garrels and Lerman, 1981, 1984; Berner and Raiswell, 1983; Berner, 1987, 2006; Kampschulte et al., 2001; Canfield, 2004; Kampschulte and Strauss, 2004). This latter response occurs in part because of the large magnitude isotope effects associated with the process of pyrite formation and burial. Constraints on the magnitude of the fractionation between oceanic sulfate and buried pyrite ($\Delta^{34}\text{S}_{\text{py}} = \delta^{34}\text{S}_{\text{seawater_sulfate}} - \delta^{34}\text{S}_{\text{buried_pyrite}}$) are therefore an important part of all of these models and carry implications for the predictions that they make.

Estimates of the magnitude of the isotope fractionation associated with pyrite formation and burial ($\Delta^{34}\text{S}_{\text{py}}$) have been obtained in a variety of different ways. These include assigning values on the basis of what is known from laboratory culture experiments with microbes that reduce sulfate (e.g., Garrels and Lerman, 1984), assigning values on the basis of studies of sedimentary pyrite and sulfate from the geologic record (e.g., Strauss, 1999; Canfield, 2004; Kampschulte and Strauss, 2004), assigning values on the basis of inferred dependences on atmospheric oxygen and model calculations (Berner, 2001), and using relationships between $^{34}\text{S}/^{32}\text{S}$ and $^{33}\text{S}/^{32}\text{S}$ for marine sulfate (Ono et al., 2006).

Here, we explore the constraints on $\Delta^{34}\text{S}_{\text{py}}$ over the course of the Phanerozoic. We examine the implications for $\Delta^{34}\text{S}_{\text{py}}$ that are provided by an analysis of the $\delta^{34}\text{S}$ record of marine sulfate and sedimentary pyrite, and we compare this to results that are obtained using methods that draw on the $\Delta^{33}\text{S}$ of seawater sulfate proxies that are independent of the $\delta^{34}\text{S}$ of buried sedimentary pyrite. We also explore how the $\Delta^{34}\text{S}_{\text{py}}$ evolution that we calibrate carries through to estimates of the sulfur sinks with time as well as to their implications for the mechanisms that control the magnitude of $\Delta^{34}\text{S}_{\text{py}}$.

2. ANALYTICAL METHODS

2.1. Isotopic analyses

As a part of this study, we report data for $\delta^{34}\text{S}$ and $\Delta^{33}\text{S}$ for a subset of the Kampschulte and Strauss (2004) sample set (Table 1), Cambrian samples from the Kuljumbe section in northwestern Siberia (Ebner et al., 1994), and Triassic samples from sections in Italy, Hungary and Slovakia (Korte, 1999). We worked with archived extracts of structurally substituted sulfate in carbonate from the Kampschulte and Strauss (2004) study.

Kampschulte and Strauss (2004) extracted sulfate from ~ 0.5 to 1 g of biogenic carbonate or ~ 200 g of micritic carbonate samples after removing the weathered portion of samples. This carbonate was crushed in an agate mill and the powdered material was soaked in a 10% NaCl solution for 24 h in order to leach water-soluble sulfate; the treated samples were rinsed with deionized water and immediately digested in 6 N HCl to extract structurally substituted sulfate which was subsequently precipitated as barium sulfate (Kampschulte et al., 2001; Kampschulte and Strauss, 2004).

The barium sulfate precipitates were reduced to hydrogen sulfide (H_2S) using a heated and actively purged (by nitrogen gas) solution of $\text{HI} + \text{H}_3\text{PO}_2 + \text{HCl}$ (Thode et al., 1961). Product hydrogen sulfide was carried in a stream of nitrogen through a water-cooled condenser and then passed through a water trap filled with Milli-Q water to remove chloride and chemically trapped as silver sulfide using 14 mL of a ~ 0.02 M solution of silver nitrate solution with 2 mL of 1.55 M HNO_3 . The solution with precipitated silver sulfide was aged in the dark for ~ 7 days, then filtered and rinsed with ~ 250 mL Milli-Q water and ~ 5 mL of 1 N ammonia water (NH_4OH). We age the samples to allow for the dissolution of an oxygen-bearing contaminant that precipitates with the silver sulfide when Thode reductions are carried out. The black precipitate of Ag_2S was collected and transferred to an aluminum packet and dried in the oven for ~ 48 h.

Samples of approximately 3 mg of silver sulfide wrapped in aluminum foil were loaded into a nickel metal vessel, which was subsequently filled with fluorine gas and heated at ~ 250 °C overnight to produce the analyte gas, sulfur hexafluoride SF_6 . The SF_6 gas was purified using cryogenic distillation in a cold trap at ~ -110 to -115 °C and further purified through gas chromatography system using one 1/8 in. OD, 4.8 m Haysep Q column with a helium flow rate of 20 mL/min. SF_6 gas was frozen into two glass traps out of the carrier helium flow and was subsequently transferred to a sample tube connected with the mass spectrometry system. The sulfur isotopic analyses were conducted using a Thermo-Finnigan MAT 253 at the stable isotope laboratory of the University of Maryland at College Park. This instrument has four collectors for simultaneous detection of ion beams with mass/charge of 127, 128, 129, and 131 Da ($^{32}\text{SF}_5^+$, $^{33}\text{SF}_5^+$, $^{34}\text{SF}_5^+$, $^{36}\text{SF}_5^+$, respectively).

We report sulfur isotope compositions using conventional delta notation (see Footnote 1). Nine analyses of IAEA-S2 which were undertaken over the course of this study yielded $\delta^{34}\text{S} = 22.23 \pm 0.16\text{‰}$, $\Delta^{33}\text{S} = 0.042 \pm$

¹ Following provisional IUPAC recommendations (Coplen, 2008), we define $\delta^{3x}\text{S}$ as $(^{3x}\text{S}/^{32}\text{S})_{\text{sample}} / (^{3x}\text{S}/^{32}\text{S})_{\text{reference}} - 1$. We define $\Delta^{33}\text{S}$ as $\delta^{33}\text{S} - ((1 + \delta^{34}\text{S})^{0.515} - 1)$ and $\Delta^{36}\text{S}$ as $\delta^{36}\text{S} - ((1 + \delta^{34}\text{S})^{1.9} - 1)$ also without the factor of 1000 with the ‰. Note that the value of $\Delta^{33}\text{S}$ we report is approximately 0.01‰ lower than that reported by Ono et al. (2006), which reflects the standardization of the two labs relative to measurements of CDT.

Table 1
Sulfur isotope data for carbonate associated sulfate.

Sample No.	Age (Ma)	Epoch	Stage	Biozone	Locality	$\delta^{34}\text{S}$ (‰, VCDT)	$\Delta^{33}\text{S}$ (‰, VCDT)
Tr49	211.8	Tr3	Nor	<i>Pargvigondolella andrusovi</i>	Slovakia	19.59	0.037
Tr55	213.3	Tr3	Nor	<i>Mockina bidentata</i>	Slovakia	19.79	0.009
Tr61	214.7	Tr3	Nor	<i>Mockina Postera</i>	Slovakia	18.18	0.018
Tr64	218.8	Tr3	Nor	<i>Epigondolella triangularis</i>	Slovakia	18.81	0.012
Tr75	224.2	Tr3	Crn	<i>Epigondolella pseudodiebeli</i>	Slovakia	20.04	0.027
Tr77	224.7	Tr3	Crn	<i>Epigondolella nodosa</i>	Slovakia	19.08	-0.008
Tr150	236.2	Tr2	Lad	<i>Budurovignathus mungoensis</i>	Hungary	18.00	0.033
Tr239	241.2	Tr1	Spa	<i>Chiosella gondolelloides</i>	Italy	27.82	0.023
Tr245	241.4	Tr1	Spa	<i>Neospathodus sosioensis</i>	Italy	27.60	0.038
Tr252	244.4	Tr1	Gri	<i>Neospathodus dieneri</i>	Italy	17.01	0.041
Tr253	244.8	Tr1	Gri	<i>Hindeodus postparvus</i>	Italy	17.25	0.038
Tr256	244.9	Tr1	Gri	<i>Isarcicella isarcica</i>	Italy	24.52	0.066
KKU-71	510.3	Mer	Dol		Siberia	37.91	-0.001
KKU-57	511.7	Mer	Dol	<i>Dolgeuloma Kaninia</i>	Siberia	29.57	-0.007
KKU-53	512.9	Mer	Dol	<i>Kujandaspis</i>	Siberia	29.49	-0.023
KKU-43	518.1	StD	Men	<i>Maspakites Idahoia Raashellina</i>	Siberia	35.23	-0.050
KKU-17	557.4	Crf	Tom	<i>Judomia Uktaspis</i>	Siberia	31.94	-0.002
KKU-4	561.3	Crf	Tom	<i>Dokidocyathus regularis</i>	Siberia	38.63	0.016

0.018‰, and $\Delta^{36}\text{S} = -0.27 \pm 0.16\text{‰}$ (all 2σ) which is comparable to a separate set of analyses conducted at the University of Maryland and reported in Ono et al. (2006) which yielded $\delta^{34}\text{S} = 22.33 \pm 0.36\text{‰}$, $\Delta^{33}\text{S} = 0.040 \pm 0.012\text{‰}$, and $\Delta^{36}\text{S} = 0.06 \pm 0.38\text{‰}$ (all 2σ) (see also Footnote 1). Uncertainty associated with the analyses for $\delta^{34}\text{S}$ and $\Delta^{33}\text{S}$ are estimated to be similar to those reported above for analyses of IAEA-S2 undertaken in this study. Our analyses of IAEA-S1 at the University of Maryland yield $\delta^{34}\text{S} = -0.3\text{‰}$, $\Delta^{33}\text{S} = 0.094\text{‰}$, and $\Delta^{36}\text{S} = -0.69\text{‰}$.

2.2. Data compilation

We also report evolution curves for the composition of sedimentary sulfide through time (assumed to be representative of buried pyrite), and for seawater sulfate. We use a compilation of the literature data (Canfield, 2005; Canfield and Farquhar, 2009) for $\delta^{34}\text{S}$ of sulfate and sulfide (Fig. 1) to derive curves that describe our estimates of the evolution of seawater sulfate and sedimentary sulfide. These curves were produced using an inverse square smoothing of the measurements and interpolated using a cubic spline.² For some of the calculations done in this study, we also use the derivatives with respect to time of the sulfate concentration. These derivatives were calculated from the smoothed curves.

Constraints on the $\Delta^{33}\text{S}$ of seawater sulfate (Fig. 2: Appendix) are derived from a combination of the results of analyses presented herein for the Cambrian, which is treated as a smoothed function for the time interval from 510 to 545 Ma, for the Triassic which is treated as a single value (0.028‰), and for previously published data presented in Johnston et al. (2005a) (Cambrian) and Doma-

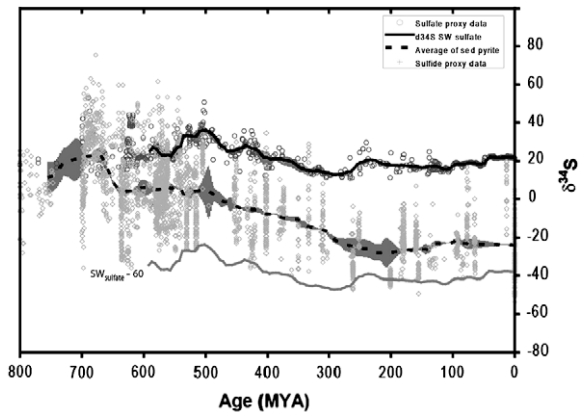


Fig. 1. Plot of $\delta^{34}\text{S}$ versus age for seawater sulfate dataset (gray unfilled circles), seawater sulfate curve (solid black line) used in calculations, sedimentary sulfide dataset (gray unfilled diamond symbols) and sedimentary sulfide curve (dashed black curve). The gray envelopes around the seawater sulfate curve and the sedimentary sulfide curve are the estimates of uncertainty used in the calculations. The solid gray curves are offset from the seawater sulfate curve by 60‰. Data are collected from Anderson and Kruger (1987), Anderson et al. (1989), Beier and Feldman (1991), Beier and Hayes (1989), Bottomley et al. (1992), Bottrell and Morton (1992), Bottrell and Raiswell (1989), Briggs et al. (1991, 1996), Burnie et al. (1972), Canfield and Farquhar (2009), Coveney and Shaffer (1988), Dill and Neilsen (1986), Dinur et al. (1980), Fike and Grotzinger (2008), Fisher (1986), Fisher and Hudson (1987), Gautier (1985a,b), Geldsetzer et al. (1987), Gorjan et al. (2000), Hattori et al. (1983), Hurtgen et al. (2006), Jowett et al. (1991), Kajiwara and Kaiho (1992), Knoll (1992), Logan et al. (1999), Marowsky (1969), Murowchick et al. (1994), Prokoph et al. (2008), Railsbeck (1989), Raiswell et al. (1993), Rickard et al. (1979), Ripley and Nicol (1981), Ross et al. (1995), Schmitz et al. (1988), Strauss et al. (1992), Underwood and Bottrell (1994), Whittaker and Kyser (1990), and Zaback and Pratt (1992).

² We have also undertaken other interpolations using various smoothing functions and have found that the results are not significantly different. Uncertainties were estimated on the basis of the residuals from the linear interpolations.

gal-Goldman et al. (2008) (Pennsylvanian), as well as in Rouxel et al. (2008) (Jurassic). The $\Delta^{33}\text{S}$ of present-day

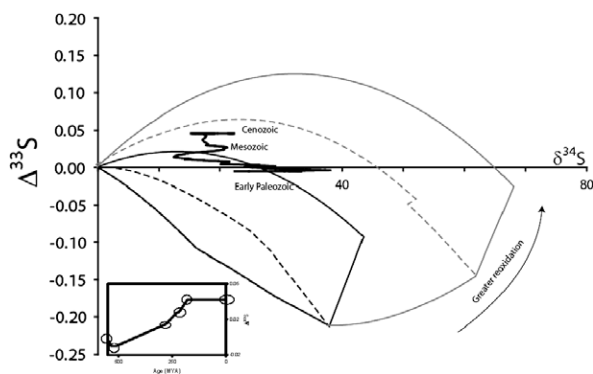


Fig. 2. Plot of $\Delta^{33}\text{S}$ versus $\delta^{34}\text{S}$ with the field of results plotted for sulfur cycle models like those presented in Johnston et al. (2005a), but with updated fractionations. The field outlined in black is for sulfate reduction only. The field outlined in gray is for sulfate reduction plus reoxidation and sulfur disproportionation. The smaller dashed fields are the fields presented in Johnston et al. (2005a). The heavy black curve describes the evolution of seawater sulfate used in this study. Note that this evolution may change as additional data and data for variations collected at higher frequency are collected. Inset is plot of $\Delta^{33}\text{S}$ versus age with circled areas representing intervals constrained by measurements.

seawater sulfate is taken to be an average of analyses of IAEA-S2 and NBS-127 undertaken at UMCP (Table 2), but this is also similar to data previously presented in Ono et al. (2006) when corrected for a difference in laboratory calibration of CDT.

3. RESULTS

Our sulfur isotope data are presented in Table 1. The Triassic sulfur isotope data are derived from 12 whole rock carbonates with the range of 17.01–27.82‰ and are comparable to previous analyses of these samples (Kampschulte and Strauss, 2004). All our Triassic sulfur isotopic data are consistent with this part of the Phanerozoic record, ex-

Table 2
Analyses of IAEA-S2 and NBS-127.

Lab #	Sample	$\delta^{33}\text{S}$	$\delta^{34}\text{S}$	$\delta^{36}\text{S}$	$\Delta^{33}\text{S}$	$\Delta^{36}\text{S}$
SF3557	IAEA-S2	11.41	22.20	42.37	0.038	-0.23
SF3613	IAEA-S2	11.41	22.21	42.33	0.036	-0.30
SF3635	IAEA-S2	11.36	22.09	42.16	0.048	-0.23
SF3661	IAEA-S2	11.37	22.13	42.20	0.036	-0.26
SF4094	IAEA-S2	11.48	22.30	42.67	0.056	-0.13
SF4104	IAEA-S2	11.43	22.22	42.33	0.044	-0.32
SF4114	IAEA-S2	11.45	22.31	42.47	0.024	-0.34
SF4123	IAEA-S2	11.47	22.30	42.42	0.047	-0.39
SF4140	IAEA-S2	11.47	22.30	42.58	0.050	-0.21
SF2394	NBS-127	10.86	21.16	40.42	0.023	-0.16
SF2437	NBS-127	10.94	21.29	40.74	0.027	-0.10
SF2499	NBS-127	10.84	21.08	40.39	0.032	-0.05
SF2500	NBS-127	10.81	21.01	40.33	0.049	0.04
SF2519	NBS-127	10.87	21.10	40.45	0.056	-0.03
SF2543	NBS-127	10.83	21.05	40.37	0.046	-0.01
SF2544	NBS-127	10.87	21.12	40.57	0.051	0.06
SF2589	NBS-127	10.83	21.04	40.01	0.051	-0.35
SF3182	NBS-127	10.83	21.09	39.94	0.027	-0.52

cept three samples, which are Tr239, Tr245, and Tr256. These three data points show higher $\delta^{34}\text{S}$ values that are attributed either to the local depositional environment or record high frequency events. The $\Delta^{33}\text{S}$ of the Triassic samples that we measured yield a range of -0.008‰ to 0.066‰ and an average of $0.028 \pm 0.038\text{‰}$ (2 SD).

The Cambrian sulfur isotope data yield a range of $\delta^{34}\text{S}$ value from 29.49‰ to 38.63‰ and $\Delta^{33}\text{S}$ from -0.050‰ to 0.016‰ and an average of $-0.011 \pm 0.046\text{‰}$ (2 SD). When combined with data previously measured in our laboratory and published in Johnston et al. (2005a,b), we observe an average $\Delta^{33}\text{S}$ of $-0.006 \pm 0.036\text{‰}$ (2 SD) for Cambrian samples which, like the Triassic samples, has a larger standard deviation than would be predicted on the basis of our estimates of analytical uncertainty.

4. DISCUSSION

4.1. Calibration of $\Delta^{34}\text{S}_{\text{py}}$ using sedimentary sulfide and sulfate

Fig. 1 presents data and curves that describe the record of seawater sulfate and sedimentary sulfide $\delta^{34}\text{S}$ values. Prior studies have observed that sedimentary sulfide data describe a minimum limit of the same shape as the seawater sulfate curve, but that is offset by approximately 60‰ to more negative $\delta^{34}\text{S}$ values (e.g., Canfield and Teske, 1996). This maximum observed fractionation between sulfate and sulfide ($\Delta^{34}\text{S}_{\text{max}}$) appears to be constant throughout the record and has been used in some studies to make arguments about the magnitude of the fractionation associated with pyrite burial (e.g., Canfield and Teske, 1996; Canfield and Raiswell, 1999). Some workers have also used this as a basis for assigning constant, high values ($\sim 50\text{‰}$) for $\Delta^{34}\text{S}_{\text{py}}$ in sulfur cycle models (e.g., Kampschulte and Strauss, 2004).

On the other hand, other workers have argued that the average value for $\delta^{34}\text{S}$ of sedimentary sulfide should represent the isotopic composition of the buried pyrite (Canfield, 2004), and that $\Delta^{34}\text{S}_{\text{py}}$ should be assigned to be approximately equal to the arithmetic difference between seawater sulfate and average sedimentary pyrite ($\delta^{34}\text{S}_{\text{sw-sulfate}} - \delta^{34}\text{S}_{\text{py-avg}}$); the difference between the two regressed curves in Fig. 1. If we take this approach, we find that the data imply a change in the magnitude of $\Delta^{34}\text{S}_{\text{py}}$ from values of about $45 \pm 5\text{‰}$ in the time since the Permian–Triassic boundary, and $30 \pm 5\text{‰}$ in the interval extending from the Cambrian through the Permian (Fig. 3). Fig. 3 also presents other histories of $\Delta^{34}\text{S}_{\text{py}}$ that have been used in other studies (e.g., Garrels and Lerman, 1984; Kurtz et al., 2003; Berner, 2004; Kampschulte and Strauss, 2004) and obtained by other ways.

If we look more closely at these calculations, we see that the arithmetic difference approach makes an assumption that the average of $\delta^{34}\text{S}$ values calculated from the sedimentary record is representative of the buried pyrite reservoir and that there are no other major sinks of sulfur with large associated isotope effects. We may then ask ourselves: How good are these assumptions? And if they are valid, is there strong enough evidence for a change in the fractionation

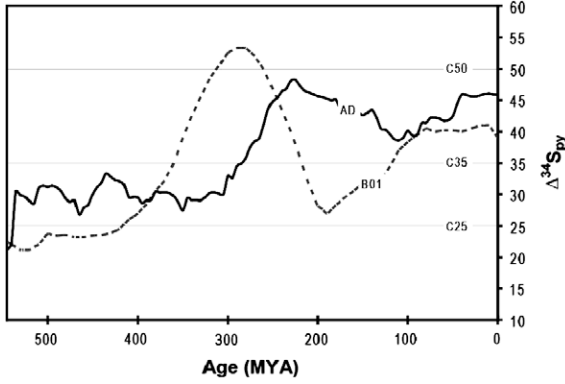


Fig. 3. Plot of curves for $\Delta^{34}\text{S}_{\text{py}}$ versus age. Three gray dotted lines labeled Constant_50, Constant_35, and Constant_25 represent values used in studies that assume a constant values for $\Delta^{34}\text{S}_{\text{py}}$ versus age. Gray dashed curve labeled BO1 is similar to one used in Berner (2001), his $J = 3$, $n = 0.5$ curve for a dependence of $\Delta^{34}\text{S}_{\text{py}}$ on atmospheric oxygen content. Black solid line is the arithmetic difference between $\delta^{34}\text{S}$ of sulfate and contemporaneous pyrite (from curves in Fig. 1). These curves are used in subsequent analysis.

associated with buried pyrite over the course of the Phanerozoic?

A number of studies have argued that the principal sink for nonsulfate sulfur is associated with pyrite burial and have not considered possibility of an unidentified sink for nonsulfate sulfur with a large associated sulfur isotope fractionation (e.g., Claypool et al., 1980; Garrels and Lerman, 1981, 1984; Berner and Raiswell, 1983; Berner, 1987, 2006; Kampschulte et al., 2001; Canfield, 2004; Kampschulte and Strauss, 2004). Several other studies (Zaback and Pratt, 1992; Werne et al., 2004; Bottrell and Newton, 2006) have made the point that the burial of organic sulfur may constitute a significant unaccounted for sink for sulfur that is fractionated relative to sulfate, and this might also influence the fractionation between pyrite and sulfate so that the isotope and mass-balance constraints do not match by a two component unmixing model. We will investigate the fractionation between pyrite and sulfate as well as the possibility of an unidentified nonsulfate sink further using methods that draw on $\Delta^{33}\text{S}$ and $\delta^{34}\text{S}$ of seawater sulfate.

4.2. Calibration of $\Delta^{34}\text{S}_{\text{py}}$ using $\Delta^{33}\text{S}$

Ono et al. (2006) have shown that it is possible to use the $\Delta^{33}\text{S}$ and $\delta^{34}\text{S}$ of seawater sulfate and a sulfur cycle model to determine $\Delta^{34}\text{S}_{\text{py}}$, provided one has constraints on the relationship between fractionations involving ^{34}S , ^{33}S , and ^{32}S . We expand this approach and use a system of equations similar to those described elsewhere (e.g., Garrels and Lerman, 1981, 1984; Berner and Raiswell, 1983; Kampschulte and Strauss, 2004) but solve in terms of R ($^{34}\text{S}/^{32}\text{S}$) and $\alpha_{a-b}(=R_a/R_b)$ rather than δ and $\Delta_{a-b}(\delta_a - \delta_b)$.³

³ This is done to facilitate coupling of the equations for $^{33}\text{S}/^{32}\text{S}$ with those for $^{34}\text{S}/^{32}\text{S}$ and the reasons for this are described in Farquhar et al. (2003, 2007). See Appendix for a derivation.

We use the standard equation to describe conservation of mass:

$$\frac{dM}{dt} = f_{\text{ew}} + f_{\text{pw}} + f_{\text{j}} - f_{\text{pb}} - f_{\text{eb}}, \quad (1)$$

where M refers to the moles of the oceanic dissolved sulfate, f_{ew} is the influx of sulfur from weathering of evaporites, f_{pw} is the influx of sulfate from oxidation of sedimentary pyrite, f_{j} is the flux of sulfur from juvenile sources (mid-ocean ridge hydrothermal sources, terrestrial volcanics, submarine eruptions), f_{pb} is the flux of sulfur lost to burial of pyrite in sediments, and f_{eb} is the flux of sulfur lost to other sources such as evaporites and carbonate associated sulfate. We use the superscript 32 (below) to indicate that this refers to the mass or flux of ^{32}S .⁴

We write an equation describing the isotope balance in terms of isotope ratios ($^{34}R_{\text{sw}} = ^{34}M/^{32}M = ^{34}\text{S}/^{32}\text{S}$) associated with the sulfur pools as:

$$\frac{d(^{34}R_{\text{sw}}^{32}M)}{dt} = ^{32}f_{\text{ew}}^{34}R_{\text{ew}} + ^{32}f_{\text{pw}}^{34}R_{\text{pw}} + ^{32}f_{\text{j}}^{34}R_{\text{j}} - ^{32}f_{\text{pb}}^{34}R_{\text{pb}} - ^{32}f_{\text{eb}}^{34}R_{\text{eb}}. \quad (2)$$

where $^{34}R_{\text{sw}}$ is the sulfur isotopic composition of dissolved sulfate and $^{34}R_{\text{ew}}$, $^{34}R_{\text{pw}}$, $^{34}R_{\text{j}}$, $^{34}R_{\text{pb}}$, and $^{34}R_{\text{eb}}$ represent the isotopic ratios of sulfur associated with the fluxes entering and leaving the oceanic sulfate pool.

The mass balance and isotope balance equations can be combined using: $\frac{d(^{34}R_{\text{sw}}^{32}M)}{dt} = ^{32}M \frac{d(^{34}R_{\text{sw}})}{dt} + ^{34}R_{\text{sw}} \frac{d(^{32}M)}{dt}$, $\alpha = \frac{^{34}R_{\text{pb}}}{^{34}R_{\text{sw}}}$, and noting $^{34}R_{\text{eb}} = ^{34}R_{\text{sw}}$ to yield:

$$^{32}M \frac{d(^{34}R_{\text{sw}})}{dt} = \left(\sum ^{32}f_n (^{34}R_n - ^{34}R_{\text{sw}}) \right) - ^{32}f_{\text{pb}}^{34}R_{\text{sw}} (\alpha - 1), \quad (3)$$

where the subscript n refers to the input fluxes (ew, pw, and j). Similar equations can be written for $^{33}R = ^{33}M/^{32}M$ using $^{33}\alpha = \alpha^\lambda$, e.g.,

$$^{32}M \frac{d(^{33}R_{\text{sw}})}{dt} = \left(\sum ^{32}f_n (^{33}R_n - ^{33}R_{\text{sw}}) \right) - ^{32}f_{\text{pb}}^{33}R_{\text{sw}} (\alpha^\lambda - 1). \quad (4)$$

These equations can then be combined to yield:

$$\frac{(\alpha^\lambda - 1)}{(\alpha - 1)} = \frac{^{34}R_{\text{sw}} \left(\frac{d(^{33}R_{\text{sw}})}{dt} - \frac{(\sum ^{32}f_n (^{33}R_n - ^{33}R_{\text{sw}}))}{^{32}M} \right)}{^{33}R_{\text{sw}} \left(\frac{d(^{34}R_{\text{sw}})}{dt} - \frac{(\sum ^{32}f_n (^{34}R_n - ^{34}R_{\text{sw}}))}{^{32}M} \right)}, \quad (5)$$

which describes the relationship between α and λ . The solution of this equation requires a number of constraints on fluxes, isotopic compositions associated with the fluxes and on the isotopic composition and mass of the seawater sulfate pool.

For calculations presented below, we use the interpolation described in Fig. 1 and the curve described in Fig. 2 (values in Appendix Table A1) for the isotopic evolution of seawater sulfate (R_{sw} and $d(R_{\text{sw}})/dt$). The isotopic

⁴ See Appendix for derivations of equations with respect to total sulfur.

composition of the flux from weathering products ($\delta^{34}\text{S}_{\text{ew}}$, $\Delta^{33}\text{S}_{\text{ew}}$, and $\delta^{34}\text{S}_{\text{pw}}$) is also derived from these curves using reasoning similar to that presented in Berner (1987),⁵ and referred to as flux parameterization 1 (FPI) in the text. The $\Delta^{33}\text{S}_{\text{pw}}$ (sulfide weathering) was estimated using an empirical relationship ($\Delta^{33}\text{S}_{\text{pw}} = -0.00221\delta^{34}\text{S}_{\text{pw}} + 0.0449$) that was derived by regressions of published and unpublished data for sedimentary sulfides (Johnston et al., 2005a, 2006, 2008; Farquhar et al., 2008). For this parameterization we assigned $\delta^{34}\text{S}_j$ to be 2‰ and with a $\Delta^{33}\text{S}$ of 0‰. The choice of $\delta^{34}\text{S}_j = 2\text{‰}$ is somewhat arbitrary, but chosen to match Kampschulte and Strauss (2004). The choice of $\Delta^{33}\text{S} = 0\text{‰}$ is chosen, assuming that the composition of juvenile sulfur is similar to CDT. The evolution of the mass of sulfate in the ocean was given by the sulfate concentration model of Lowenstein et al. (2003). The flux of sulfur from juvenile sources (f_j) was set to an estimate of the present-day flux (5.0×10^{11} mol/yr – Canfield, 2004) and made proportional to the normalized amount of crust production (Gaffin, 1987) for times in the past. For the parameterization of sources of sulfate (juvenile sulfur, evaporite weathering, and pyrite weathering) we used two different parameterizations to represent the range of values that have been used. For the first of these, which refer to as FPI we used values of fluxes into the system that are similar to those used by Kampschulte and Strauss (2004). For the second parameterization (FP2) we used values of source fluxes that are similar to those used/derived by Berner (2004).

4.2.1. Calibration of λ and $\Delta^{34}\text{S}_{\text{py}}$

If we consider Eq. (5), we see that in order to determine the value of $\Delta^{34}\text{S}_{\text{py}}$, one needs a constraint on λ . This was recognized by Ono et al. (2006) who used assumptions about the probable values of λ to calibrate $\Delta^{34}\text{S}_{\text{py}}$. In principle, one could also assign $\Delta^{34}\text{S}_{\text{py}}$ and use Eq. (5) to constrain λ ; or if another relationship could be found that describes the way that $\Delta^{34}\text{S}_{\text{py}}$ and λ covary, $\Delta^{34}\text{S}_{\text{py}}$ and λ could be simultaneously determined by combining Eq. (5) with such a relationship.

With Fig. 3 we illustrated several different model curves that have been used in prior studies for the evolution of $\Delta^{34}\text{S}_{\text{py}}$. These model curves include those that assume a constant value of $\Delta^{34}\text{S}_{\text{py}}$ for the entire Phanerozoic, as well

⁵ For a given point in time in the Phanerozoic record we reconstruct the composition of the weathering products from the values in Table A1 using equal proportions of a component that has a short residence time (10 My for sulfate and 25 My for sulfide) and a component that has a longer residence time (40 My for sulfate and 200 My for sulfide). The compositions of these components are determined by taking running averages. The timescales for evaporite weathering are similar to the timescales for high frequency and lower frequency sea level oscillations (e.g., Haq and Schutter, 2008). Sea level oscillations may allow for accumulation of evaporites in low lying arid zones during regressive phases and discharges (flux) of sulfate to the oceanic pool by flooding during transgressive phases, in much the same way that a capacitor stores electric charge. When discharged, this evaporite ‘flux capacitor’ transfers sulfate back to the continents where it is stored for future release.

as curves that assume more complicated variation with time and include: (1) a model curve that is calculated as the arithmetic difference between the seawater curve and the average of sedimentary pyrite (AD); and (2) a model curve that deviates from this and is assigned on other grounds, including a dependence of $\Delta^{34}\text{S}_{\text{py}}$ on atmospheric oxygen concentration (BO1) (Berner, 2001).

Fig. 4 presents the calculated results for λ using the $\Delta^{34}\text{S}_{\text{py}}$ evolution presented in Fig. 3 and the sulfur cycle model described by Eq. (5). Different evolution of λ is shown for FPI and FP2 scenarios, the reason for this can be seen by examining Eq. (5). The right hand side of Eq. (5) relates a number of measured or assigned parameters such as the composition of seawater sulfate ($^{33}R_{\text{sw}}$ and $^{34}R_{\text{sw}}$) and the variability of isotope ratios of seawater sulfate as a result of reservoir effects scaled by the size of the sulfate pool ($^{32}M \frac{d(^{33}R_{\text{sw}})}{dt}$) and ($^{32}M \frac{d(^{34}R_{\text{sw}})}{dt}$), to the composition of the sulfate source fluxes into the oceans ($\sum ^{32}f_n(^{33}R_n - ^{33}R_{\text{sw}})$) and ($\sum ^{32}f_n(R_n - R_{\text{sw}})$). We solve the right hand side of Eq. (5) by assigning values to each

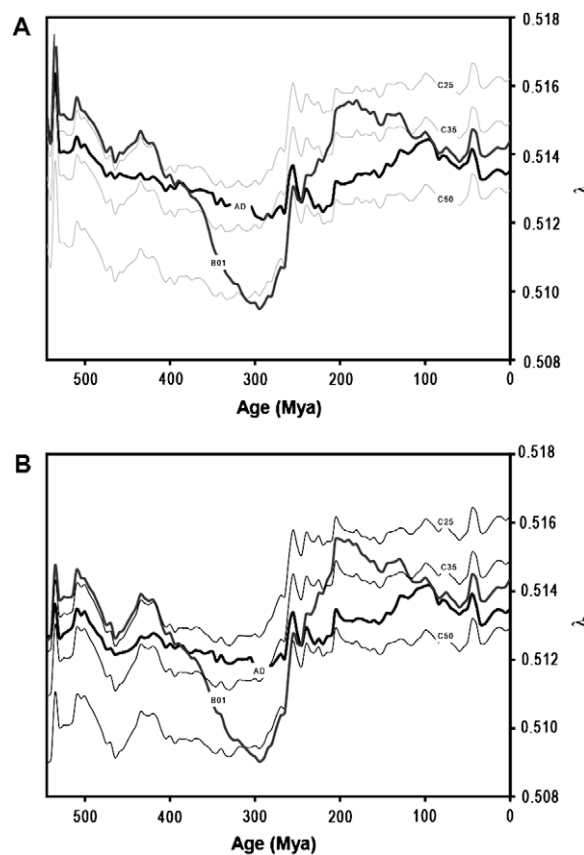


Fig. 4. Plot of curves of λ versus age calculated with the FPI parameterization (A) and the FP2 parameterization (B) for the $\Delta^{34}\text{S}_{\text{py}}$ versus age curves in Fig. 3. Three gray thin lines labeled C50, C35, and C25 are calculated using constant values for $\Delta^{34}\text{S}_{\text{py}}$ versus age of 50‰, 35‰, and 25‰. Gray curve labeled BO1 used the $\Delta^{34}\text{S}_{\text{py}}$ versus age given in Berner (2001), his $J = 3$, $n = 0.5$ curve for a dependence of $\Delta^{34}\text{S}_{\text{py}}$ on atmospheric oxygen content. Black solid line uses the $\Delta^{34}\text{S}_{\text{py}}$ versus age given by the arithmetic difference between $\delta^{34}\text{S}$ of sulfate and contemporaneous pyrite (from curves in Fig. 1).

of these variables. This yields a result that is solved for α and λ using the left hand side of Eq. (5). This does not provide a way to determine whether one calculation of λ with time is better than the other. There are recent determinations of λ using observations from the geologic record. They focus on values of λ which are derived from regression of the isotopic data of sedimentary pyrite rather than sulfate–sulfide pairs. The results of these regressions yield (0.5127 ± 0.0003) for Proterozoic to Phanerozoic sediments and (0.5138 ± 0.0009) for modern sediments (values reported in Johnston et al., 2008). If these are the relevant values for λ (~ 0.513 – 0.514), they are satisfied for the Phanerozoic only by the curve calculated using the arithmetic difference between the seawater and sedimentary sulfide (Fig. 4a), but this in itself does not constitute an irrefutable argument in support of this calibration of $\Delta^{34}\text{S}_{\text{py}}$ and λ .

To explore this further, we define a relationship between α and λ that releases us from the need for making a direct assignment of either $\Delta^{34}\text{S}_{\text{py}}$ or λ . Recent studies have examined the way that the fractionations for $^{34}\text{S}/^{32}\text{S}$ $^{33}\text{S}/^{32}\text{S}$ are related for sulfate-reducing, sulfur-disproportionating, and sulfide oxidizing bacteria (e.g., Farquhar et al., 2003, 2007, 2008; Johnston et al., 2005a,b, 2007, 2008; Zerkle et al., 2009) and the results of these studies can be used to calibrate a relationship that describes the way that α and λ $\Delta^{34}\text{S}_{\text{py}}$ and λ may covary in the sulfur cycle. We do this by using a sulfur cycle box model like that presented in Fig. 5 and by solving for the fractionation between the sulfate pool and the buried pyrite pool as a function of the proportions of sulfur reduced directly to pyrite and of sulfide oxidized and disproportionated. The equation that describes this relationship is:

$$\alpha_{\text{py}} = \frac{R_{\text{sulfate}}}{R_{\text{pyrite}}} = \frac{f_{\text{reox}}[(f_{\text{disp}}\alpha_{\text{disp}} - (1 - f_{\text{disp}})\alpha_{\text{reox}}) - 1] + 1}{\alpha_{\text{sr}}}, \quad (6)$$

where α_{py} is the fractionation factor between sulfate and pyrite, α_{disp} ⁶ is the fractionation factor associated with disproportionation, α_{sr} is the fractionation factor associated with sulfate reduction, and α_{s_i} is the fractionation factor associated with oxidation of sulfide to the sulfur intermediate pool. The terms f_{s_i} and f_{disp} are the fractions of ^{32}S in the sulfide pool that are reoxidized to sulfate, and fraction of the reoxidized ^{32}S that is subject to disproportionation.⁷ An explanation of the derivation of this equation is given in Appendix.

We use this equation and constraints from all available sulfate reduction data (except those for the thermophile *Archaeoglobus. fulgidus*), sulfur disproportionation data, and sulfide oxidation data (Johnston et al., 2005a,b, 2007;

Farquhar et al., 2008; Zerkle et al., 2009) to define a field of fractionations between sulfate and buried pyrite as a function of the fraction of sulfide that is reoxidized and disproportionated (given in Fig. 6A). For this plot the role of disproportionation increases moving toward the right hand side of the field (compositions with higher $\Delta^{34}\text{S}_{\text{py}}$ and λ , and the role of sulfate reduction (without reoxidation and disproportionation) is higher in the left hand side.

Eq. (5) provides a relationship between $\Delta^{34}\text{S}_{\text{py}}$ and λ which trend from the lower right to upper left in Fig. 6. The intersections of these solutions and the field in Fig. 6A are given in Fig. 6B (gray shaded area) and represent the collection of solutions that satisfy the sulfur cycle inversion of Eq. (5) and the box model given in Appendix Eq. (A.6). We have also grouped these solutions into averages for 50 million year intervals for parameterizations *FPI* and *FP2* (black and gray dashed lines). These results further support a change in the fractionation associated with pyrite burial between 200 and 300 Mya and are consistent with an increase in the $\Delta^{34}\text{S}_{\text{py}}$ and/or λ associated with pyrite burial and with an increase with time in the proportion of sulfur cycled through disproportionation. The field in Fig. 6B is also consistent with only two of models for the evolution of $\Delta^{34}\text{S}_{\text{py}}$, the constant $\Delta^{34}\text{S}_{\text{py}}$ of 35‰ and the $\Delta^{34}\text{S}_{\text{py}}$ given by the arithmetic difference method. It is not clear, whether one or neither of these models is to be preferred. In Fig. 6C we give the results of the arithmetic difference method (see triangle symbols) using both *FPI* and *FP2*.

There are a number of possible ways that $\Delta^{34}\text{S}_{\text{py}}$ and λ may have varied other than those given by the arithmetic difference method or by assuming a constant $\Delta^{34}\text{S}_{\text{py}}$, or λ . One approach that we investigate next explores the possibility that this evolution can be described using a single set of fractionations (invariant) for sulfate reduction, and by varying the proportion of sulfide reoxidation and sulfur disproportionation, whose fractionations are also fixed. In this case, all of the variation for $\Delta^{34}\text{S}_{\text{py}}$ and λ results from changes in the proportion of reoxidation and disproportionation. For this calculation (which is illustrated in Fig. 6C – circle symbols), we use the average values of the experiments with sulfate reducers, sulfur disproportionators (elemental S) and two fractionations for sulfide oxidation (values and reference presented in Appendix Table A4).

Fig. 7A and B illustrate the variation of $\Delta^{34}\text{S}_{\text{py}}$ and λ with geologic time for the full field of solutions constrained by the model, the results of the arithmetic difference method, and for the calculation just described that assumes a single set of biological fractionations. The range in results arises mostly from the variability in sulfate reduction fractionation that we have measured in laboratory experiments (see Fig. 6A). These figures also illustrate common features of all of these solutions. All are consistent with a change in the values of $\Delta^{34}\text{S}_{\text{py}}$ (and in some cases λ) from lower values in the early Phanerozoic and higher values since about 200 million years ago. All of these results imply a fundamental change in the way that sulfur isotopes were fractionated in the sulfur cycle. Average values for $\Delta^{34}\text{S}_{\text{py}}$ and λ provided by the these models are presented in Table 3 and suggest a change in the magnitude of $\Delta^{34}\text{S}_{\text{py}}$ from values of

⁶ In the case of the fractionation factor for disproportionation, we use the same approach that was used in Johnston et al. (2005a), that involve calculating the net fractionation associated with sulfur disproportionation by a combined pathway.

⁷ We use ^{32}S instead of total sulfur because it provides an exact solution for the equation, and introduces only a small approximation to calculations made using total sulfur. See Farquhar et al. (2007) for a discussion of this approach.

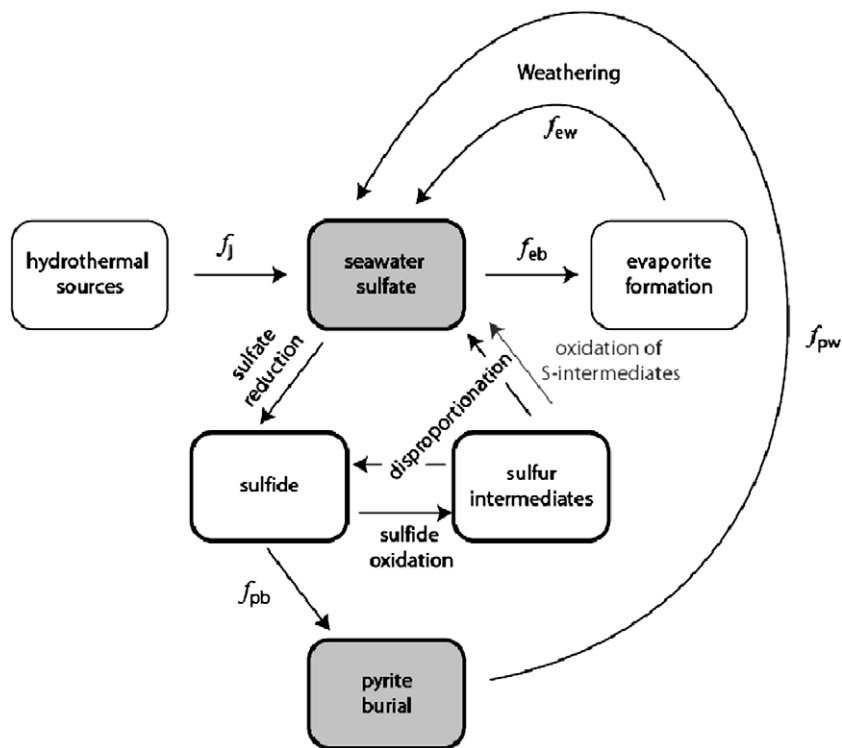


Fig. 5. Schematic diagram of sulfur cycle box model used to calculate the fractionation between seawater sulfate and pyrite burial. This model consists of six sulfur pools (labeled boxes) and various transformations of sulfur that result in mass transfer between pools (black and gray arrows). The model is a modification of models used in Zerkle et al. (2009) and Johnston et al. (2005a).

approximately 30‰ in the Paleozoic to values of approximately 41‰ since 200 million years ago and a similar change in values of λ from values of ~ 0.5128 to values of ~ 0.5138 in these same time intervals. It is not clear at present which evolution of $\Delta^{34}\text{S}_{\text{py}}$ and λ (the arithmetic difference method or the method that assumes a single set of fractionations for sulfate reduction, sulfide oxidation and disproportionation) is closer to capturing the true nature of the variation in $\Delta^{34}\text{S}_{\text{py}}$ and λ , but this should become apparent with future work.

4.3. Implications of a change in $\Delta^{34}\text{S}_{\text{py}}$ and λ for the sulfur cycle

Given the context provided by prior studies of the sulfur cycle (cf., Johnston et al., 2005a, 2006), the change from smaller $\Delta^{34}\text{S}_{\text{py}}$ values and lower λ values in the Paleozoic to higher values for both quantities starting in the Mesozoic and carrying through to the Cenozoic, suggests a change in the sulfur cycle that would include a more prominent role for disproportionation in the latter parts of the Phanerozoic (Fig. 6B). The reason for this change is not clear, but it does imply a change in the reoxidative pathways for sulfur.

In Fig. 8, we plot an array of panels that illustrate the way that $\Delta^{34}\text{S}_{\text{py}}$ factors into determinations of pyrite burial flux estimates (Fig. 8A, D, and G), evaporite burial flux estimates (Fig. 8B, E, and H) and the proportional amount of pyrite burial relative to other sinks (Fig. 8C, F, and I). These panels illustrate how using higher values for $\Delta^{34}\text{S}_{\text{py}}$

yield smaller magnitude estimates of the pyrite burial flux (and larger evaporite burial flux estimates), while using lower values for $\Delta^{34}\text{S}_{\text{py}}$ yield larger magnitude estimates for the pyrite burial flux. These panels also illustrate how choosing low values for $\Delta^{34}\text{S}_{\text{py}}$ yields a larger dynamic range (point to point variability) for estimates of the burial flux and for estimates of the ratio of pyrite burial to the total sulfur sinks (F_{py}).

Panels A, B, and C were calculated using input flux parameterization FP1 (similar to those used in Kampschulte and Strauss, 2004) and panels D, E, and F were calculated using input flux parameterization FP2 (similar to those used in Berner, 2004). The clear difference between panels A, B, and C relative to panels D, E, and F illustrates the dependence of output fluxes on the choice of input fluxes. The dependence is most pronounced for estimates of the ratio of pyrite burial to the total sulfur sinks (F_{py}), in large part because in the model we use, a change in the influx of sulfate from evaporite weathering, shifts the $\delta^{34}\text{S}$ of incoming sulfate either closer to or further from that of the standing sulfate pool. Panel F also includes an estimate of pyrite burial fraction (F_{py}) obtained using $(\delta^{34}\text{S}_{\text{sulfate}} - \delta^{34}\text{S}_{\text{input}})/(\delta^{34}\text{S}_{\text{sulfate}} - \delta^{34}\text{S}_{\text{pyrite}})$ ⁸ (thick black line) that is in better agreement with results obtained using FP2 than with those obtained using FP1.

⁸ $\delta^{34}\text{S}_{\text{input}}$ is the average $\delta^{34}\text{S}$ of the input sulfur (ew, pw, and j).

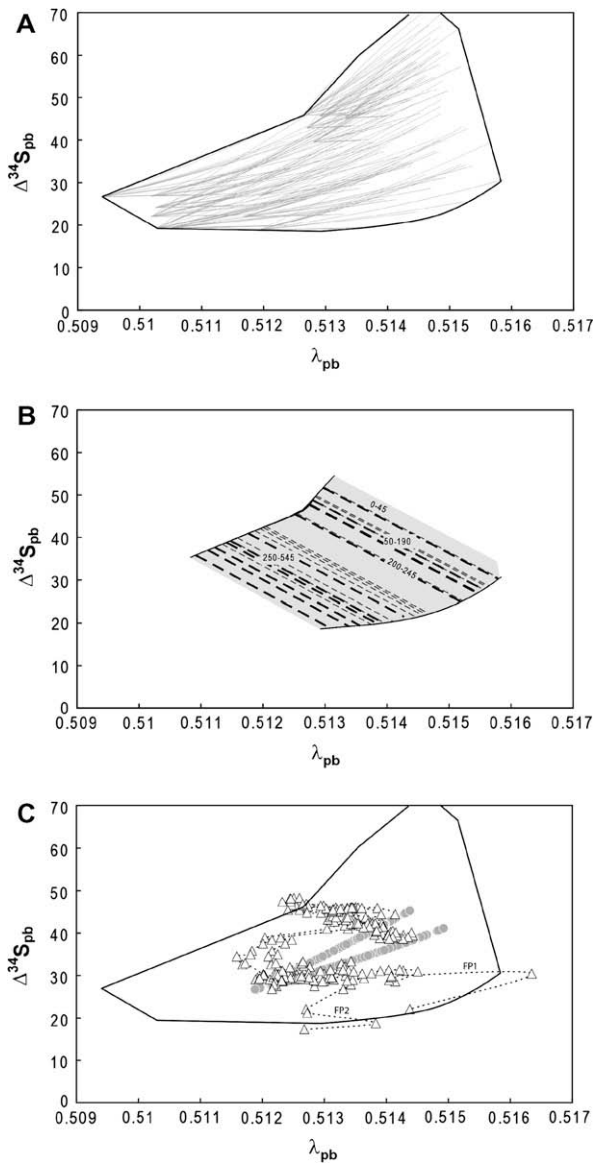


Fig. 6. (A) Plot of $\Delta^{34}\text{S}_{\text{py}}$ versus λ with outlines of the field resulting from the model in Fig. 5, calibrated with fractionations measured in laboratory culture experiments (Farquhar et al., 2003; Johnston et al., 2005b, 2007). The light gray lines are results of calculations with individual permutations of laboratory data. (B) The gray field is defined by the intersection of results of model calculations using Eq. (5) and calculations of the relationship between $\Delta^{34}\text{S}_{\text{py}}$ and λ in (A). The dashed lines are the solutions averaged on a 50 My time intervals throughout the Phanerozoic using FP1 (gray) and FP2 (black). (C) Plot of data for the arithmetic difference between sulfate and sulfide (λ calculated from Eq. (5)) for FP1 and FP2 (triangles connected by dotted line) and for solutions constrained by average fractionations for sulfate reduction, elemental sulfur disproportionation and sulfide oxidation (circles) for which the two arrays are calculated using two different fractionation factors for sulfide oxidation ($\sim -7\text{‰}$ and $+1.5\text{‰}$) similar to those reported in Fry et al. (1984) and Zerkle et al. (2009) for abiotic and phototrophic oxidation pathways.

Results obtained using the ^{33}S method with *FP1* and *FP2* are presented in panels G–I, and are broadly consistent with the ensemble of solutions presented in panels A–F. The results obtained using the ^{33}S method exhibit a broad range of values, and those obtained using the *FP2* parameterization bear a weak resemblance to other model curves for the Phanerozoic (e.g., Lowenstein et al., 2003; Berner, 2004) and also model curves for sea floor production rates (e.g., Gaffin, 1987) and sea level (Haq and Schutter, 2008). Part of this similarity (e.g., for evaporite burial) is imposed by the chosen values for the sulfur input fluxes, but we believe that part of this is also independent of the input constraints (e.g., for pyrite burial and to a lesser extent for F_{py}). Similar (albeit muted) features are observed when *FP1* is used and these appear to be related in part to the general shape of the curve that describes the average $\delta^{34}\text{S}$ of sedimentary pyrite. We suggest that this may reflect underlying connections between pyrite burial, the area of continental shelves and sea level fluctuations similar to those suggested for other element cycles (e.g., Bjerrum et al., 2006). The submerging of 30–40% of the present-day emergent continental area would more than triple the area of the continental shelves. Even taking into account the reduction in sulfate reduction rates and pyrite burial because of greater depth and distance from the shorelines, the addition of these loci for pyrite burial would be anticipated to have an effect.

4.4. A note on the possible role of organic sulfur burial in the sulfur cycle and its bearing on estimates of $\Delta^{34}\text{S}_{\text{py}}$ and λ

The sulfur cycle model that we have used to extract estimates of $\Delta^{34}\text{S}_{\text{py}}$ and λ includes only one sink associated with fractionated sulfur (pyrite sulfur–sulfide). Other sinks for sulfur may exist at some times in earth’s history associated with burial of organic sulfur. Zaback and Pratt (1992) and more recently, Werne et al. (2004) and Bottrell and Newton (2006) have argued that the burial of organic sulfur during some times in Earth history (e.g., the Miocene) may have been significant, *and that* the isotopic composition of this sulfur will be different (more ^{34}S -enriched) than that of the pyrite sink. We have not taken this possibility into consideration in an explicit way with the present treatment. In principle it should manifest itself as a mismatch between the $\Delta^{34}\text{S}_{\text{py}}$ determined by the arithmetic difference method and the $\Delta^{34}\text{S}_{\text{py}}$ determined by the methods used here that call upon $\Delta^{33}\text{S}$ and sulfur cycle models. These latter methods should capture the combination of all highly fractionated nonsulfate sinks (pyrite, organic S, and any other unidentified sinks). The correspondence between results obtained using these two methods suggests that the general long-term implications for $\Delta^{34}\text{S}_{\text{py}}$ and λ are valid, and that there is not a significant long-term missing nonsulfate sulfur sink that is highly fractionated. This result is however *only as good* as the sampling density that we presently have and our results do not rule out the possibility that an organic S sink may have been important at some times in the Phanerozoic. Our methods in fact provide a way to search for evidence of this sink by future, higher-resolution studies.

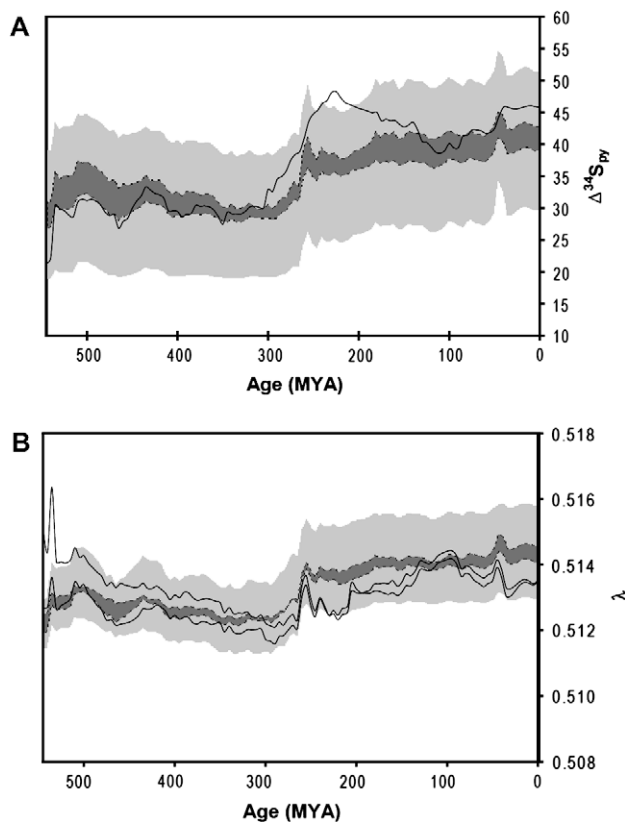


Fig. 7. Plots of (A) $\Delta^{34}\text{S}_{\text{py}}$ versus age and (B) λ versus age. Light gray field is field of full solutions given by the intersection of results of model calculations using Eq. (5) and calculations of the relationship between $\Delta^{34}\text{S}_{\text{py}}$ and λ (also plotted in Fig. 6B). Darker gray field illustrates the intersection of results of model calculations using Eq. (5) and the relationship between $\Delta^{34}\text{S}_{\text{py}}$ and λ given by the average fractionations for sulfate reduction, elemental sulfur disproportionation and sulfide oxidation. Black lines are solutions calculated for the FP1 and FP2 parameterizations using the arithmetic difference between $\delta^{34}\text{S}$ of sulfate and contemporaneous pyrite.

Table 3
Results of model calculations for $\Delta^{34}\text{S}_{\text{py}}$ and λ .

	$\Delta^{34}\text{S}$ (average)	SD ^a	λ (average)	SD
<i>0–200 Mya</i>				
Full field of solutions ^a	39	11	0.5142	0.0014
Arithmetic difference method ($\delta_{\text{sw}} - \delta_{\text{sed}}$)	43	2	0.5136	0.0004
Single fractionation method	40	2	0.5141	0.0003
<i>300–545 Mya</i>				
Full field of solutions ^a	31	10	0.5129	0.0012
Arithmetic difference method ($\delta_{\text{sw}} - \delta_{\text{sed}}$)	30	2	0.5129	0.0007
Single fractionation method	31	2	0.5127	0.0004

^a For full field of solutions this is given as the range of the field.

5. SUMMARY AND CONCLUSIONS

The isotopic composition of sulfate in the oceans integrates the fractionations associated with the supply and removal of sulfur from the ocean. This composition is strongly influenced by processes such as bacterial sulfate reduction, which introduces large metabolic isotope effects (>40‰) in the product sulfide relative to reactant sulfate. Other processes that affect the isotopic composition of the sulfate pool include oxidation processes acting on sulfide to form sulfur intermediate compounds (e.g., thiosulfate, elemental sulfur, polysulfides, and polythionates), as well

as subsequent reductive, oxidative, and disproportionative biological and abiological pathways which complete the sulfur cycle (cf., Canfield, 2001). The principal controls on the isotopic composition of seawater sulfate are believed to be a combination of effects related to the sinks of sulfate (bacterial sulfate reduction and sulfur intermediate compound disproportionation) and at another level to the sources of sulfate. These two processes produce ^{32}S -enriched sulfide that is sequestered by sedimentary pyrite, and as a result of a reservoir effect, leaves the oceanic sulfate pool ^{32}S -depleted relative to its sulfur inputs. These processes also provide a link to the carbon cycle through

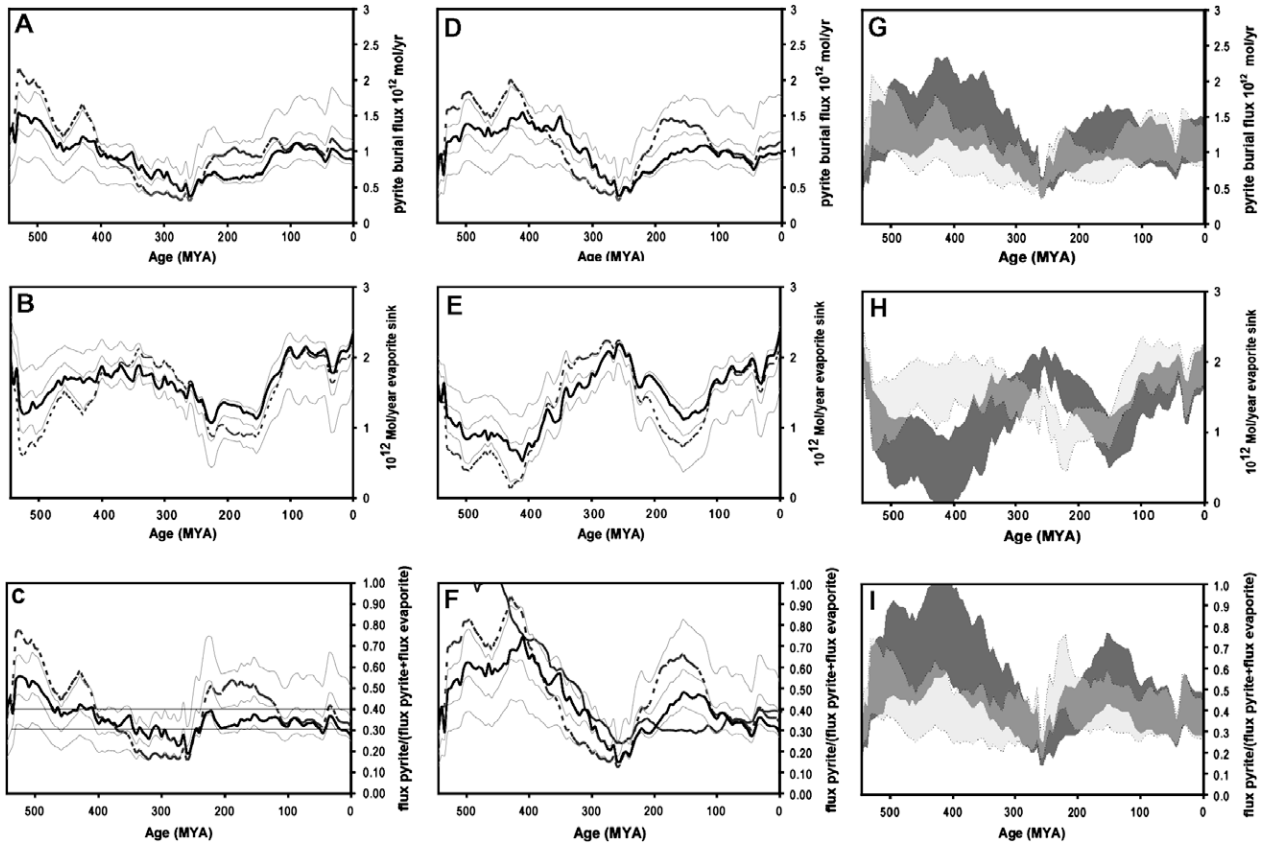


Fig. 8. Plots of model output for pyrite burial flux, evaporite burial flux, and F_{py} versus age for parameterization FP1 (A–C), FP2 (D–F) and using the ^{33}S method with both parameterizations (G and H). Curves in panels A–F are similar to those used in Fig. 4. Three gray thin lines are calculated using constant values for $\Delta^{34}\text{S}_{py}$ versus age of 50‰, 35‰, and 25‰. The higher the values for $\Delta^{34}\text{S}_{py}$ yield smaller magnitude estimates of the pyrite burial flux (and larger evaporite burial flux estimates). Gray dashed curve labeled BO1 used the $\Delta^{34}\text{S}_{py}$ versus age given in Berner (2001), his $J = 3$, $n = 0.5$ curve for a dependence of $\Delta^{34}\text{S}_{py}$ on atmospheric oxygen content. Black solid line uses the $\Delta^{34}\text{S}_{py}$ versus age given by the arithmetic difference between $\delta^{34}\text{S}$ of sulfate and contemporaneous pyrite (from curves in Fig. 1). Thick gray line in panel F is an estimate of pyrite burial fraction (F_{py}) obtained using $(\delta^{34}\text{S}_{\text{sulfate}} - \delta^{34}\text{S}_{\text{input}})/(\delta^{34}\text{S}_{\text{sulfate}} - \delta^{34}\text{S}_{\text{pyrite}})$. Darker band in panels G–I is calculated using FP2 and lighter band is calculated using FP1.

organic carbon mineralization (Jørgensen, 1982). The full complement of processes associated with sulfate reduction, sulfide oxidation and oxidation or disproportionation of sulfur intermediates operating in diagenetic and water-column environments establishes the fractionation between seawater sulfate and buried pyrite ($\Delta^{34}\text{S}_{py}$).

The analysis provided here, both with the arithmetic difference method ($\Delta^{34}\text{S}_{py} = \delta^{34}\text{S}_{sw} - \delta^{34}\text{S}_{py}$) and with independent methods that call upon $\Delta^{33}\text{S}$ and sulfur cycle models, illustrates that $\Delta^{34}\text{S}_{py}$ and λ appear to exhibit a bimodal character in the Phanerozoic, marked by a transition that starts at or near the Permian–Triassic boundary and to extend through the late Triassic. It is argued that this change is connected to a change in the ecology of the oceanic sulfur cycle, and while the origin of this change is not entirely clear, constraints can be placed on the possible causes of this change using the analysis above (Figs. 6 and 7).

- If we accept the $\Delta^{34}\text{S}_{py}$ evolution model of the arithmetic difference method, the change in Fig. 6C is implied to be the result of a shift in the fractionations associated with sulfate reduction and the fraction of sulfide that is

oxidized. This model does not rule out the possibility of changes in the fractionations associated with sulfur disproportionation of sulfide oxidation, but it also does not appear to require them.

- Alternatively, the data may be fit to a single set of fractionations for sulfate reduction, disproportionation, or sulfide oxidation, resulting in a systematic relationship between $\Delta^{34}\text{S}_{py}$ and λ that would vary as a result of changes in the fraction of sulfide that was oxidized and processed through disproportionation, and this may be a significant change. For example, using the average fractionations for sulfate reduction, S disproportionation and sulfide oxidation, yields lower limits⁹ on the estimate of the reoxidation followed by disproportionation of $\sim 72 \pm 11\%$ and $22 \pm 12\%$ for the time intervals 0–200 and 300–545 Mya, respectively.

⁹ These are lower limits because the presence of pathways for direct oxidation to sulfate will result in higher values (Zerkle et al., 2009).

- The third possibility, a constant $\Delta^{34}\text{S}_{\text{py}}$ would also imply a tightly coupled cycle with a relationship between the fractionations associated with sulfate reduction, disproportionation, and sulfide oxidation and also the fraction of sulfide oxidized that is difficult to explain.

The resolution of this question lies with further analyses of sedimentary pyrite and with experiments relating isotope effects to metabolisms relevant in the sulfur cycle. A key may be the way that $\Delta^{34}\text{S}_{\text{py}}$ and λ covary. Regardless of the specific details of the cause of the change in $\Delta^{34}\text{S}_{\text{py}}$, it seems that the change requires a more prominent role for reoxidation and disproportionation since the early Triassic.

ACKNOWLEDGMENTS

This study was supported by funds from an NSF Career Grant, a grant from the NASA exobiology program, the Danish Grundforskningsfund, and a Guggenheim Fellowship (J.F.). The authors thank Brendan Williams and Andrew Masterson for technical help. Grant # EAR0918382 provided support during revisions.

APPENDIX A. DERIVATION OF EQUATIONS IN TERMS OF TOTAL SULFUR

Notation:

Influx: $f_{\text{ew}}, f_{\text{pw}}, f_{\text{J}}$ (mol/yr)

Outflux: $f_{\text{pb}}, f_{\text{eb}}$ (mol/yr)

Ratio definition: ${}^{34}R = \frac{{}^{34}M}{{}^{32}M}$, ${}^{33}R = \frac{{}^{33}M}{{}^{32}M}$, ${}^{36}R = \frac{{}^{36}M}{{}^{32}M}$

$$\sum R = (1 + {}^{34}R + {}^{33}R + {}^{36}R)$$

$${}^{34}R_{\text{sw}} = \frac{{}^{34}M}{{}^{32}M}, \quad {}^{33}\alpha = \frac{{}^{33}R_{\text{py}}}{{}^{33}R_{\text{sw}}}, \quad {}^{34}\alpha = \frac{{}^{34}R_{\text{py}}}{{}^{34}R_{\text{sw}}}, \quad {}^{33}\alpha = {}^{34}\alpha^2$$

$$\frac{d({}^{34}R_{\text{sw}})}{dt} = \frac{d\left(\frac{{}^{34}M}{{}^{32}M}\right)}{dt} = \frac{1}{{}^{32}M} \left[\frac{d{}^{34}M}{dt} - \left(\frac{{}^{34}M}{{}^{32}M}\right) \times \frac{d{}^{32}M}{dt} \right] \quad (\text{A.1})$$

$$\frac{d({}^{33}R_{\text{sw}})}{dt} = \frac{d\left(\frac{{}^{33}M}{{}^{32}M}\right)}{dt} = \frac{1}{{}^{32}M} \left[\frac{d{}^{33}M}{dt} - \left(\frac{{}^{33}M}{{}^{32}M}\right) \times \frac{d{}^{32}M}{dt} \right] \quad (\text{A.2})$$

$$\begin{aligned} \frac{d{}^{34}M}{dt} &= \frac{{}^{34}R_{\text{ew}}}{\sum R_{\text{ew}}} \times f_{\text{ew}} + \frac{{}^{34}R_{\text{pw}}}{\sum R_{\text{pw}}} \times f_{\text{pw}} + \frac{{}^{34}R_{\text{J}}}{\sum R_{\text{J}}} \times f_{\text{J}} \\ &\quad - \frac{{}^{34}R_{\text{pb}}}{\sum R_{\text{pb}}} \times f_{\text{pb}} - \frac{{}^{34}R_{\text{eb}}}{\sum R_{\text{eb}}} \times f_{\text{eb}} \end{aligned} \quad (\text{A.3})$$

$$\begin{aligned} \frac{d{}^{33}M}{dt} &= \frac{{}^{33}R_{\text{ew}}}{\sum R_{\text{ew}}} \times f_{\text{ew}} + \frac{{}^{33}R_{\text{pw}}}{\sum R_{\text{pw}}} \times f_{\text{pw}} + \frac{{}^{33}R_{\text{J}}}{\sum R_{\text{J}}} \times f_{\text{J}} \\ &\quad - \frac{{}^{33}R_{\text{pb}}}{\sum R_{\text{pb}}} \times f_{\text{pb}} - \frac{{}^{33}R_{\text{eb}}}{\sum R_{\text{eb}}} \times f_{\text{eb}} \end{aligned} \quad (\text{A.4})$$

$$\begin{aligned} \frac{d{}^{32}M}{dt} &= \frac{1}{\sum R_{\text{ew}}} \times f_{\text{ew}} + \frac{1}{\sum R_{\text{pw}}} \times f_{\text{pw}} + \frac{1}{\sum R_{\text{J}}} \times f_{\text{J}} \\ &\quad - \frac{1}{\sum R_{\text{pb}}} \times f_{\text{pb}} - \frac{1}{\sum R_{\text{eb}}} \times f_{\text{eb}}. \end{aligned} \quad (\text{A.5})$$

Substitute Eq. (A.3) and Eq. (A.5) into Eq. (A.1) to yield:

$$\begin{aligned} {}^{32}M \times \frac{d({}^{34}R_{\text{sw}})}{dt} &= \frac{f_{\text{ew}}}{\sum R_{\text{Evap}}} \times ({}^{34}R_{\text{ew}} - {}^{34}R_{\text{sw}}) \\ &\quad + \frac{f_{\text{pw}}}{\sum R_{\text{pw}}} \times ({}^{34}R_{\text{pw}} - {}^{34}R_{\text{sw}}) \\ &\quad + \frac{f_{\text{J}}}{\sum R_{\text{J}}} \times ({}^{34}R_{\text{J}} - {}^{34}R_{\text{sw}}) \\ &\quad + \frac{f_{\text{pb}}}{\sum R_{\text{pb}}} \times ({}^{34}R_{\text{sw}} - {}^{34}R_{\text{pb}}) \end{aligned} \quad (\text{A.6-1})$$

$$\begin{aligned} {}^{32}M \times \frac{d({}^{34}R_{\text{sw}})}{dt} &= \frac{f_{\text{ew}}}{\sum R_{\text{ew}}} \times ({}^{34}R_{\text{ew}} - {}^{34}R_{\text{sw}}) \\ &\quad + \frac{f_{\text{pw}}}{\sum R_{\text{pw}}} \times ({}^{34}R_{\text{pw}} - {}^{34}R_{\text{sw}}) \\ &\quad + \frac{f_{\text{J}}}{\sum R_{\text{J}}} \times ({}^{34}R_{\text{J}} - {}^{34}R_{\text{sw}}) \\ &\quad + \frac{f_{\text{PB}} \times {}^{34}R_{\text{sw}}}{\sum R_{\text{pb}}} (1 - {}^{34}\alpha). \end{aligned} \quad (\text{A.6-2})$$

Substitute Eq. (A.4) and Eq. (A.5) into Eq. (A.2) to yield:

$$\begin{aligned} {}^{32}M \times \frac{d({}^{33}R_{\text{sw}})}{dt} &= \frac{f_{\text{ew}}}{\sum R_{\text{ew}}} \times ({}^{33}R_{\text{ew}} - {}^{33}R_{\text{sw}}) \\ &\quad + \frac{f_{\text{pw}}}{\sum R_{\text{pw}}} \times ({}^{33}R_{\text{pw}} - {}^{33}R_{\text{sw}}) \\ &\quad + \frac{f_{\text{J}}}{\sum R_{\text{J}}} \times ({}^{33}R_{\text{J}} - {}^{33}R_{\text{sw}}) \\ &\quad + \frac{f_{\text{pb}}}{\sum R_{\text{pb}}} \times ({}^{33}R_{\text{sw}} - {}^{33}R_{\text{pb}}) \end{aligned} \quad (\text{A.7-1})$$

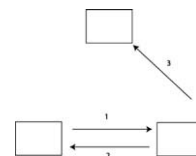
$$\begin{aligned} {}^{32}M \times \frac{d({}^{33}R_{\text{sw}})}{dt} &= \frac{f_{\text{ew}}}{\sum R_{\text{ew}}} \times ({}^{33}R_{\text{ew}} - {}^{33}R_{\text{sw}}) \\ &\quad + \frac{f_{\text{pw}}}{\sum R_{\text{pw}}} \times ({}^{33}R_{\text{pw}} - {}^{33}R_{\text{sw}}) \\ &\quad + \frac{f_{\text{J}}}{\sum R_{\text{J}}} \times ({}^{33}R_{\text{J}} - {}^{33}R_{\text{sw}}) \\ &\quad + \frac{f_{\text{pb}} \times {}^{33}R_{\text{sw}}}{\sum R_{\text{pb}}} (1 - {}^{33}\alpha). \end{aligned} \quad (\text{A.7-2})$$

Combine Eq. (A.7-1) and Eq. (A.7-2) to yield:

$$\frac{(\alpha^2 - 1)}{(\alpha - 1)} = \frac{{}^{34}R_{\text{sw}} \times \left\{ \frac{d({}^{33}R_{\text{sw}})}{dt} - \sum \frac{f_n \times ({}^{33}R_n - {}^{33}R_{\text{sw}})}{{}^{32}M \times \sum R_n} \right\}}{{}^{33}R_{\text{sw}} \times \left\{ \frac{d({}^{34}R_{\text{sw}})}{dt} - \sum \frac{f_n \times ({}^{34}R_n - {}^{34}R_{\text{sw}})}{{}^{32}M \times \sum R_n} \right\}}. \quad (\text{A.8})$$

APPENDIX B. DERIVATION OF TEXT EQ. (6)

We start the derivation of text Eq. (6) by working through the fractionation associated with oxidation followed by disproportionation.



The ratios of isotopes transferred via disproportionation can be described by:

$$R_1 = f_{D_ox}R_3 + (1 - f_{D_ox})R_2,$$

where f_{D_ox} is the fractional amount of ^{32}S that is oxidized via pathway 3 compared to the total amount of sulfur that is disproportionated. Noting that $\alpha_{\text{reox}}R_{\text{sulfide}} = R_1$, $\alpha_{D_red}R_{\text{intermediate}} = R_2$, and $\alpha_{D_ox}R_{\text{intermediate}} = R_3$, can be substituted to yield:

$$\alpha_{\text{reox}}R_{\text{sulfide}} = f_{D_ox}R_3 + (1 - f_{D_ox})\frac{\alpha_{D_red}}{\alpha_{D_ox}}R_3. \quad (\text{B.1})$$

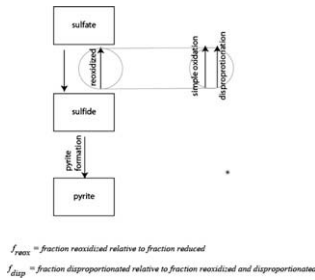
This can be rearranged to yield:

$$\frac{R_{\text{sulfide}}}{R_{\text{sulfate}}} = \frac{f_{D_ox} + (1 - f_{D_ox})\frac{\alpha_{D_red}}{\alpha_{D_ox}}}{\alpha_{\text{reox}}}. \quad (\text{B.2})$$

Following the convention $-\alpha_{\text{disp}}R_{\text{sulfide}} = R_{\text{flux_to_sulfate}}$,

$$\alpha_{\text{disp}} = \frac{\alpha_{\text{reox}}}{f_{D_ox} + (1 - f_{D_ox})\frac{\alpha_{D_red}}{\alpha_{D_ox}}}. \quad (\text{B.3})$$

The pathway described in Fig. 5 includes pathways for fractionation that are related to both disproportionation and straight reoxidation that can be described schematically as:



At steady state the ratios of isotopes moving along the oxidative paths can be described using:

$$\alpha_{\text{reox}}R_{\text{sulfide}} = f_{\text{disp}}R_{\text{flux_to_sulfate_via_disp}} + (1 - f_{\text{disp}})R_{\text{reox}}, \quad (\text{B.4})$$

where f_{disp} is the fraction of reoxidized sulfur processed by the disproportionation pathway(s). Noting that the total fractionation associated with oxidation is related to these by f_{disp} , we rewrite this equation as:

$$\alpha_{\text{total_ox}}R_{\text{sulfide}} = f_{\text{disp}}\alpha_{\text{disp}}R_{\text{sulfide}} + (1 - f_{\text{disp}})\alpha_{\text{reox}}R_{\text{sulfide}}, \quad (\text{B.5})$$

and further simplify it to:

$$\alpha_{\text{total_ox}} = f_{\text{disp}}\alpha_{\text{disp}} - (1 - f_{\text{disp}})\alpha_{\text{reox}}. \quad (\text{B.6})$$

We can then insert the equation: $\alpha_{\text{total_ox}}R_{\text{sulfide}} = R_{\text{flux_back_to_sulfate}}$ into master network along the using a branching term f_{reox} that describes the fraction of sulfide reoxidized relative to the total sulfur reduced: $\alpha_{\text{sr}}R_{\text{sulfate}} = f_{\text{reox}}\alpha_{\text{total_ox}}R_{\text{pyrite}} + (1 - f_{\text{reox}})R_{\text{pyrite}}$, and this can be expanded by substitution of (B.6) to yield:

$$\alpha_{\text{sr}}R_{\text{sulfate}} = f_{\text{reox}}(f_{\text{disp}}\alpha_{\text{disp}} - (1 - f_{\text{disp}})\alpha_{\text{reox}})R_{\text{pyrite}} + (1 - f_{\text{reox}})R_{\text{pyrite}}, \quad (\text{B.7})$$

which when rearranged yields:

$$\frac{R_{\text{sulfate}}}{R_{\text{pyrite}}} = \frac{f_{\text{reox}}(f_{\text{disp}}\alpha_{\text{disp}} - (1 - f_{\text{disp}})\alpha_{\text{reox}}) + (1 - f_{\text{reox}})}{\alpha_{\text{sr}}}. \quad (\text{B.8})$$

This can be simplified to:

$$\frac{R_{\text{sulfate}}}{R_{\text{pyrite}}} = \frac{f_{\text{reox}}[(f_{\text{disp}}\alpha_{\text{disp}} - (1 - f_{\text{disp}})\alpha_{\text{reox}}) - 1] + 1}{\alpha_{\text{sr}}}. \quad (\text{B.9})$$

Since α_{disp} is significantly larger than α_{reox} the extent of the field of solutions is given when $f_{\text{disp}} \rightarrow 1$, and this is the field that is plotted in Fig. 6. The relationship between α and λ for values of $f_{\text{disp}} < 1$ do not follow exactly the same relationship to that produced changes in f_{reox} but the changes are very small and our tests suggest they do not affect the conclusions. The solution was obtained using approaches outlined in Farquhar et al. (2007) and noting that the larger network could be built by nesting smaller subunits into the following network structure (Tables A2 and A3).

Table A1
Tabulated data used for sulfate and sulfide evolution.

Age (Mya)	$\delta^{34}\text{S}$	$\Delta^{33}\text{S}$	$\delta^{34}\text{S}$	$\Delta^{33}\text{S}$
0	21.8	0.042	-24.0	0.098
5	21.9	0.042	-24.0	0.098
10	22.1	0.042	-23.9	0.098
15	22.1	0.042	-23.9	0.099
20	21.9	0.042	-23.9	0.099
25	21.7	0.042	-23.8	0.099
30	21.8	0.042	-23.8	0.099
35	22.1	0.042	-23.7	0.099
40	22.2	0.042	-23.7	0.099
45	20.8	0.042	-23.6	0.099
50	18.9	0.042	-23.6	0.099
55	18.3	0.042	-23.5	0.099
60	18.3	0.042	-23.5	0.099
65	18.7	0.042	-23.4	0.098
70	18.9	0.042	-23.4	0.098
75	18.9	0.042	-23.3	0.098
80	18.4	0.042	-23.0	0.098
84	18.2	0.042	-23.1	0.098
90	18.5	0.042	-21.0	0.097
95	18.2	0.042	-21.2	0.098
100	17.4	0.042	-22.7	0.098
105	16.2	0.042	-22.8	0.098
110	15.7	0.042	-22.9	0.098
115	15.7	0.042	-23.1	0.099
120	16.4	0.042	-23.2	0.099
125	17.1	0.042	-23.2	0.099
130	17.3	0.042	-23.2	0.100
135	17.2	0.042	-25.1	0.100
140	17.1	0.042	-26.3	0.100
145	16.9	0.042	-26.1	0.100
150	16.5	0.042	-26.1	0.099
155	16.9	0.042	-26.2	0.099
160	17.4	0.042	-26.4	0.099
165	17.2	0.042	-26.5	0.099
170	17.3	0.042	-26.6	0.098

(continued on next page)

Table A1 (continued)

Age (Mya)	$\delta^{34}\text{S}$	$\Delta^{33}\text{S}$	$\delta^{34}\text{S}$	$\Delta^{33}\text{S}$
175	17.4	0.042	-26.3	0.098
180	17.7	0.042	-27.3	0.098
185	17.6	0.040	-27.4	0.098
190	17.8	0.038	-27.4	0.097
195	17.9	0.037	-27.6	0.097
200	17.9	0.035	-27.7	0.096
205	18.0	0.033	-27.9	0.096
210	18.1	0.031	-28.1	0.095
215	18.6	0.029	-28.0	0.094
220	19.3	0.028	-28.0	0.093
225	20.2	0.028	-28.0	0.092
230	20.5	0.027	-27.6	0.091
235	20.7	0.026	-26.2	0.090
240	20.4	0.025	-26.0	0.089
245	19.6	0.023	-25.8	0.088
250	19.2	0.022	-25.6	0.087
255	18.2	0.021	-25.5	0.086
260	16.2	0.020	-24.8	0.084
265	14.6	0.018	-24.3	0.083
270	14.4	0.017	-24.0	0.082
275	13.7	0.016	-23.8	0.080
280	13.0	0.015	-22.8	0.078
285	13.0	0.014	-22.0	0.076
290	12.8	0.013	-21.7	0.074
295	13.0	0.013	-19.6	0.072
300	13.7	0.012	-19.3	0.071
305	13.8	0.012	-16.2	0.069
310	14.2	0.011	-16.0	0.068
315	14.7	0.011	-15.6	0.067
320	14.9	0.010	-15.3	0.066
325	14.6	0.010	-14.9	0.065
330	14.7	0.009	-14.3	0.064
335	15.1	0.009	-14.0	0.063
340	15.8	0.008	-13.3	0.061
345	16.1	0.008	-13.3	0.060
350	17.0	0.007	-10.5	0.059
355	18.4	0.007	-10.3	0.058
360	19.5	0.006	-10.2	0.057
365	20.1	0.005	-10.1	0.057
370	20.3	0.005	-10.0	0.056
375	20.6	0.004	-9.7	0.055
380	21.2	0.004	-9.2	0.054
385	21.3	0.003	-7.9	0.053
390	21.2	0.003	-7.8	0.052
395	20.9	0.002	-7.8	0.052
400	21.7	0.002	-7.7	0.051
405	21.9	0.001	-7.6	0.050
410	23.6	0.001	-6.0	0.049
415	25.6	0.000	-5.9	0.049
420	26.5	0.000	-5.5	0.048
425	26.9	-0.001	-5.4	0.048
430	27.6	-0.002	-5.2	0.047
435	28.2	-0.002	-5.1	0.046
440	27.0	-0.003	-4.9	0.045
445	26.5	-0.003	-4.6	0.044
450	26.0	-0.004	-4.0	0.043
455	25.4	-0.004	-3.0	0.042
460	25.4	-0.005	-2.5	0.040

Table A1 (continued)

Age (Mya)	$\delta^{34}\text{S}$	$\Delta^{33}\text{S}$	$\delta^{34}\text{S}$	$\Delta^{33}\text{S}$
465	25.3	-0.005	-1.5	0.039
470	27.4	-0.006	-1.6	0.037
475	28.1	-0.006	-0.7	0.035
480	30.5	-0.007	1.1	0.034
485	32.4	-0.007	1.9	0.032
490	34.0	-0.008	2.9	0.031
495	35.2	-0.009	3.8	0.031
500	36.1	-0.009	4.9	0.030
505	35.9	-0.010	4.5	0.030
510	35.3	-0.010	4.3	0.030
515	32.7	-0.010	4.1	0.029
520	32.7	-0.010	3.8	0.029
525	33.0	-0.010	3.4	0.028
530	33.1	-0.010	3.2	0.027
535	32.8	-0.010	2.4	0.026
540	27.7	-0.007	5.6	0.025
545	27.1	-0.006	5.8	0.025
550	25.3	-0.002	6.4	0.025
555	22.6	-0.001	5.2	0.025
560	23.1	-0.001	6.4	0.025
565	23.0	-0.001	7.2	0.025
570	23.0	-0.001	5.7	0.025
575	24.5	-0.001	4.9	0.025
580	26.3	-0.002	4.9	0.024
585	27.1	-0.002	5.4	0.024
590	25.3	-0.002	5.5	0.024
595	24.3	-0.003	6.0	0.025
600			5.9	0.025
605			5.9	0.025
610			4.5	0.025
615			4.4	0.025
620			4.2	0.024
625			4.1	0.023
630			3.9	0.021
635			3.9	0.018
640			5.2	0.014
645			7.0	0.011
650			9.3	0.007
655			13.7	0.005
660			17.3	0.003
665			20.9	0.002
670			23.5	0.002
675			23.3	0.002
680			23.1	0.003
685			22.8	0.004
691			22.6	0.005
695			22.2	0.005
700			21.9	0.006
705			21.5	0.007
710			21.0	0.000
715			20.5	0.000
720			20.2	0.000
725			20.1	0.000
730			19.6	0.000
735			16.6	0.000
740			13.6	0.000
745			12.2	0.000
750			11.7	0.000
755			11.3	0.000

Table A2
Of inputs and results for model FPI.

Age (Mya)	Flux juvenile sulfur (10^{12} mol/yr)	Flux evaporite weathering (10^{12} mol/yr)	Flux pyrite weathering (10^{12} mol/yr)
0	0.50	1.30	0.65
5	0.51	1.33	0.67
10	0.53	1.36	0.68
15	0.54	1.39	0.70
20	0.55	1.42	0.71
25	0.57	1.45	0.73
30	0.58	1.45	0.73
35	0.59	1.46	0.73
40	0.61	1.46	0.73
45	0.62	1.46	0.73
50	0.63	1.46	0.73
55	0.67	1.46	0.73
60	0.70	1.46	0.73
65	0.73	1.46	0.73
70	0.76	1.46	0.73
75	0.79	1.45	0.73
80	0.80	1.45	0.73
84	0.81	1.46	0.73
90	0.82	1.46	0.73
95	0.83	1.46	0.73
100	0.83	1.46	0.73
105	0.83	1.43	0.71
110	0.83	1.39	0.70
115	0.86	1.36	0.68
120	0.87	1.32	0.66
125	0.85	1.29	0.64
130	0.83	1.23	0.61
135	0.77	1.17	0.58
140	0.71	1.11	0.55
145	0.63	1.05	0.53
150	0.60	0.99	0.50
155	0.55	0.99	0.49
160	0.57	0.98	0.49
165	0.58	0.97	0.48
170	0.57	0.96	0.48
175	0.57	0.95	0.47
180	0.56	0.96	0.48
185	0.55	0.96	0.48
190	0.55	0.97	0.49
195	0.54	0.98	0.49
200	0.53	0.98	0.49
205	0.54	0.99	0.50
210	0.55	1.00	0.50
215	0.55	1.01	0.51
220	0.56	1.02	0.51
225	0.57	1.03	0.51
230	0.56	1.01	0.51
235	0.55	1.00	0.50
240	0.55	0.98	0.49
245	0.54	0.97	0.48
250	0.53	0.95	0.47
255	0.57	0.95	0.47
260	0.57	0.94	0.47
265	0.57	0.94	0.47
270	0.57	0.93	0.47

Table A2 (*continued*)

Age (Mya)	Flux juvenile sulfur (10^{12} mol/yr)	Flux evaporite weathering (10^{12} mol/yr)	Flux pyrite weathering (10^{12} mol/yr)
275	0.60	0.93	0.46
280	0.62	0.97	0.48
285	0.63	1.00	0.50
290	0.61	1.04	0.52
295	0.59	1.08	0.54
300	0.58	1.12	0.56
305	0.54	1.12	0.56
310	0.53	1.12	0.56
315	0.51	1.12	0.56
320	0.55	1.12	0.56
325	0.58	1.12	0.56
330	0.62	1.12	0.56
335	0.66	1.12	0.56
340	0.69	1.12	0.56
345	0.70	1.12	0.56
350	0.70	1.12	0.56
355	0.70	1.13	0.56
360	0.69	1.14	0.57
365	0.69	1.14	0.57
370	0.69	1.15	0.57
375	0.68	1.15	0.58
380	0.68	1.21	0.60
385	0.68	1.26	0.63
390	0.67	1.32	0.66
395	0.67	1.37	0.69
400	0.67	1.43	0.72
405	0.68	1.43	0.71
410	0.69	1.42	0.71
415	0.71	1.41	0.71
420	0.72	1.40	0.70
425	0.73	1.39	0.70
430	0.73	1.38	0.69
435	0.73	1.36	0.68
440	0.72	1.34	0.67
445	0.72	1.33	0.66
450	0.72	1.31	0.65
455	0.72	1.31	0.66
460	0.72	1.32	0.66
465	0.72	1.32	0.66
470	0.72	1.33	0.66
475	0.73	1.33	0.66
480	0.73	1.34	0.67
485	0.73	1.36	0.68
490	0.73	1.37	0.68
495	0.73	1.38	0.69
500	0.73	1.39	0.70
505	0.75	1.38	0.69
510	0.80	1.36	0.68
515	0.81	1.35	0.67
520	0.81	1.33	0.67
525	0.83	1.32	0.66
530	0.77	1.45	0.72
535	0.70	1.58	0.79
540	0.50	1.70	0.85
545	0.50	1.83	0.91

Table A3

Of inputs and results for model FP2.

Age (Mya)	Flux juvenile sulfur (10^{12} mol/yr)	Flux evaporite weathering (10^{12} mol/yr)	Flux pyrite weathering (10^{12} mol/yr)
0	0.25	1.50	0.85
5	0.22	1.49	0.88
10	0.19	1.50	0.89
15	0.20	1.52	0.89
20	0.21	1.55	0.89
25	0.11	1.59	0.88
30	0.00	1.63	0.87
35	0.04	1.66	0.86
40	0.08	1.68	0.85
45	0.04	1.68	0.85
50	0.00	1.66	0.86
55	0.02	1.64	0.87
60	0.03	1.63	0.87
65	0.04	1.61	0.87
70	0.05	1.60	0.88
75	0.11	1.59	0.89
80	0.16	1.58	0.90
84	0.11	1.57	0.91
90	0.06	1.56	0.92
95	0.03	1.54	0.94
100	0.00	1.52	0.96
105	0.04	1.49	0.98
110	0.08	1.45	0.99
115	0.05	1.42	1.01
120	0.02	1.38	1.03
125	0.01	1.33	1.04
130	0.00	1.30	1.05
135	0.00	1.29	1.06
140	0.00	1.30	1.06
145	0.01	1.30	1.07
150	0.02	1.30	1.07
155	0.00	1.31	1.07
160	0.00	1.33	1.06
165	0.00	1.36	1.05
170	0.00	1.38	1.03
175	0.00	1.40	1.02
180	0.00	1.42	1.00
185	0.00	1.47	0.98
190	0.00	1.53	0.95
195	0.00	1.58	0.91
200	0.00	1.63	0.87
205	0.00	1.67	0.83
210	0.00	1.71	0.80
215	0.00	1.76	0.78
220	0.00	1.81	0.75
225	0.00	1.87	0.71
230	0.00	1.93	0.65
235	0.00	1.98	0.58
240	0.00	2.00	0.54
245	0.01	1.98	0.54
250	0.12	1.93	0.57
255	0.10	1.88	0.61
260	0.08	1.83	0.64
265	0.13	1.78	0.67
270	0.18	1.73	0.70

Table A3 (*continued*)

Age (Mya)	Flux juvenile sulfur (10^{12} mol/yr)	Flux evaporite weathering (10^{12} mol/yr)	Flux pyrite weathering (10^{12} mol/yr)
275	0.22	1.68	0.74
280	0.27	1.63	0.78
285	0.17	1.57	0.82
290	0.06	1.51	0.86
295	0.09	1.44	0.90
300	0.12	1.37	0.95
305	0.21	1.28	0.99
310	0.30	1.18	1.04
315	0.28	1.11	1.10
320	0.26	1.05	1.15
325	0.23	1.00	1.20
330	0.20	0.95	1.24
335	0.31	0.88	1.29
340	0.42	0.80	1.34
345	0.32	0.74	1.39
350	0.23	0.70	1.44
355	0.11	0.66	1.48
360	0.00	0.64	1.50
365	0.09	0.60	1.51
370	0.18	0.57	1.51
375	0.11	0.53	1.53
380	0.03	0.50	1.55
385	0.04	0.47	1.57
390	0.06	0.45	1.59
395	0.09	0.43	1.62
400	0.12	0.42	1.64
405	0.09	0.41	1.65
410	0.05	0.41	1.65
415	0.04	0.41	1.65
420	0.03	0.42	1.65
425	0.03	0.43	1.65
430	0.02	0.44	1.65
435	0.00	0.45	1.63
440	0.00	0.47	1.62
445	0.00	0.49	1.61
450	0.00	0.51	1.59
455	0.00	0.53	1.57
460	0.00	0.55	1.56
465	0.00	0.59	1.55
470	0.00	0.62	1.54
475	0.00	0.64	1.53
480	0.00	0.67	1.51
485	0.00	0.71	1.48
490	0.03	0.75	1.46
495	0.04	0.77	1.45
500	0.04	0.80	1.44
505	0.02	0.86	1.41
510	0.00	0.93	1.37
515	0.00	0.99	1.34
520	0.00	1.05	1.31
525	0.00	1.11	1.26
530	0.00	1.18	1.21
535	0.00	1.24	1.17
540	0.00	1.30	1.13
545	0.00	1.35	1.07

Table A4
Fractionation factors used models.

	alpha 34	alpha 33
J2005/7	0.985778	0.992719
J2005/7	0.981102	0.990280
J2005/7	0.978011	0.988687
J2005/7	0.980266	0.989879
J2005/7	0.977844	0.988633
F2008	0.956350	0.977369
F2008	0.956189	0.977296
F2008	0.958961	0.978744
F2008	0.956768	0.977569
F2008	0.961999	0.980329
J2007	0.974045	0.986694
J2007	0.973876	0.986585
J2007	0.976403	0.987889
J2007	0.980976	0.990242
Average	0.973766	0.986483
SO3 J2005/7	0.969598	0.984177
SO3 J2005/7	0.970583	0.984708
SO3 J2005/7	0.946291	0.971996
SO3 J2005/7	0.955693	0.976941
Average	0.973296	0.986081
S J2005/7	0.975442	0.987184
S J2005/7	0.971150	0.984977
Average	0.960541	0.979456
Chem. F86EST	0.993000	0.996389
Biol. F86EST, Z09	1.001500	1.000772

Citations:

J2005/7: Johnston et al. (2005a,b) modified in Johnston et al. (2007).
 J2007: Johnston et al. (2007).
 F2008: Farquhar et al. (2008).
 F86EST: ³⁴S alpha estimated on the basis of Fry et al., 1984, 1988.
 Z09: Zerkle et al. (2009).

REFERENCES

- Anderson T. F. and Kruger J. (1987) C–S–Fe relationships and the isotopic composition of pyrite in the New Albany of the Illinois Basin, U.S.A.. *Geochim. Cosmochim. Acta* **51**, 2795–2805.
- Anderson I. K., Andrew C. J., Ashton J. H., Boyce A. J., Caulfield J. B. D., Fallick A. E. and Russell M. J. (1989) Preliminary sulphur isotope data of diagenetic and vein sulphides in the Lower Palaeozoic strata of Ireland and Southern Scotland: implications for Zn + Pb + Ba mineralization. *J. Geol. Soc. Lond.* **146**, 715–720.
- Beier J. A. and Feldman H. R. (1991) Sulfur isotopes and paragenesis of sulfide minerals in the Silurian Waldron Shale, southern Indiana. *Geology* **19**, 389–392.
- Beier J. A. and Hayes J. M. (1989) Geochemical and isotopic evidence for paleoredox conditions during deposition of the Devonian–Mississippian New Albany Shale, southern Indiana. *Geol. Soc. Am. Bull.* **101**, 774–782.
- Berner R. A. (1987) Models for carbon and sulfur cycles and atmospheric oxygen: application to Paleozoic geologic history. *Am. J. Sci.* **287**, 177–196.
- Berner R. A. (2001) Modeling atmospheric O₂ over Phanerozoic time. *Geochim. Cosmochim. Acta* **65**, 685–694.
- Berner R. A. (2004) A model for calcium, magnesium and sulfate in seawater over Phanerozoic time. *Am. J. Sci.* **304**, 438–453.
- Berner R. A. (2006) GEOCARBSULF: a combined model for Phanerozoic atmospheric O₂ and CO₂. *Geochim. Cosmochim. Acta* **70**, 5653–5664.
- Berner R. A. and Raiswell R. (1983) Burial of organic carbon and pyrite sulfur in sediments over Phanerozoic time: a new theory. *Geochim. Cosmochim. Acta* **47**, 855–862.
- Bjerrum C. J., Bendtsen J. and Legarth J. J. F. (2006) Modeling organic carbon burial during sea level rise with reference to the Cretaceous. *Geochem. Geophys. Geosyst.* **7**. doi:10.1029/2005GC001032.
- Bottomley D. J., Veizer J., Nielsen H. and Moczydlowska M. (1992) Isotopic composition of disseminated sulfur in Precambrian sedimentary rocks. *Geochim. Cosmochim. Acta* **56**, 3311–3322.
- Bottrell S. H. and Morton M. D. B. (1992) A reinterpretation of the genesis of the Cae Coch pyrite deposit, North Wales. *J. Geol. Soc. Lond.* **149**, 581–584.
- Bottrell S. H. and Newton R. J. (2006) Reconstruction of changes in global sulfur cycling from marine sulfate isotopes. *Earth Sci. Rev.* **75**, 59–83.
- Bottrell S. and Raiswell R. (1989) Primary versus diagenetic origin of Blue Lias rhythms (Dorset, UK): evidence from sulphur geochemistry. *Terra Nova* **1**, 451–456.
- Briggs D. E. G., Bottrell S. H. and Raiswell R. (1991) Pyritization of soft-bodied fossils: Beecher's Trilobite Bed, Upper Ordovician, New York State. *Geology* **19**, 1221–1224.
- Briggs D. E. G., Raiswell R., Bottrell S. H., Hatfield D. and Bartels C. (1996) Controls on the pyritization of exceptionally preserved fossils: an analysis of the Lower Devonian Hunsrück Slate of Germany. *Am. J. Sci.* **296**, 633–663.
- Burnie S. W., Schwarcz H. P. and Crocket J. H. (1972) A sulfur isotopic study of the White Pine Mine, Michigan. *Econ. Geol.* **67**, 895–914.
- Canfield D. E. (2001) Biogeochemistry of sulfur isotopes. In *Stable Isotope Geochemistry*, vol. 43, pp. 607–636.
- Canfield D. E. (2004) The evolution of the Earth surface sulfur reservoir. *Am. J. Sci.* **304**, 839–861.
- Canfield D. E. (2005) The early history of atmospheric oxygen: Homeage to Robert M. Garrels. *Annu. Rev. Earth Planet. Sci.* **33**, 1–36.
- Canfield D. E. and Farquhar J. (2009) Animal evolution, bioturbation, and the sulfate concentration of the oceans. *Proc. Natl Acad. Sci. USA* **106**(20), 8123–8127.
- Canfield D. E. and Raiswell R. (1999) The evolution of the sulfur cycle. *Am. J. Sci.* **299**, 697–723.
- Canfield D. E. and Teske A. (1996) Late Proterozoic rise in atmospheric oxygen concentration inferred from phylogenetic and sulphur-isotope studies. *Nature* **382**(6587), 127–132.
- Claypool G. E., Holser W. T., Kaplan I. R., Sakai H. and Zak I. (1980) The age curves of sulfur and oxygen isotopes in marine sulfate and their mutual interpretation. *Chem. Geol.* **28**, 199–260.
- Coplen T. B. (2008) Explanatory Glossary of Terms Used in Expression of Relative Isotope Ratios and Gas Ratios, IUPAC Provisional Recommendations, Inorganic Chemistry Division, Commission on Isotopic Abundances and Atomic Weights. <http://old.iupac.org/reports/provisional/abstract08/coplen_310508.html>.
- Coplen T. B., Böhlke J. K., De Bièvre P., Ding T., Holden N. E., Hopple J. A., Krouse H. R., Lamberty A., Peiser H. S., Révész K., Rieder S. E., Rosman K. J. R., Roth E., Taylor P. D. P., Vocke J. R. and Xiao Y. K. (2002) Isotope-abundance variations of selected elements. *Pure Appl. Chem.* **74**, 1987–2017.
- Coveney, Jr., R. M. and Shaffer N. R. (1988) Sulfur-isotope variations in Pennsylvanian shales of the midwestern United States. *Geology* **16**, 18–21.

- Dill H. and Neilsen H. (1986) Carbon–sulphur–iron-variations and sulphur isotope patterns of Silurian Graptolite Shales. *Sedimentology* **33**, 745–755.
- Dinur D., Spiro B. and Aizenshtat Z. (1980) The distribution and isotopic composition of sulfur in organic-rich sedimentary rocks. *Chem. Geol.* **31**, 37–51.
- Domagal-Goldman S. D., Kasting J. F., Johnston D. T. and Farquhar J. (2008) Using multiple sulfur isotopes to constrain Archean atmosphere. *Earth Planet. Sci. Lett.* **269**, 29–40.
- Ebneth S., Strauss H., Gravestock D. I. and Veizer J. (1994) Carbon isotope stratigraphy of the Lower Cambrian: new data from South Australia and Siberia. In *Ecological Aspects of the Cambrian Radiation (IGSP 366)*. *Terra Nova Abstract Supplement*, vol. 3, p. 3.
- Farquhar J., Johnston D. T., Wing B. A., Habicht K. S., Canfield D. E., Airieau S. and Thiemens M. H. (2003) Multiple sulfur isotopic interpretations of biosynthetic pathways: implications for biological signatures in the sulfur isotope record. *Geobiology* **1**, 27–36.
- Farquhar J., Johnston D. T. and Wing B. A. (2007) Influence of network structure on sulfur isotope phase space of dissimilatory sulfate reduction: implications of conservation of mass effects on mass-dependent isotope fractionations. *Geochim. Cosmochim. Acta* **71**, 5862–5875.
- Farquhar J., Canfield D. E., Masterson A. J. and Johnston D. T. (2008) Sulfur and oxygen isotope study of sulfate reduction in experiments with natural populations from Fællestrand, Denmark. *Geochim. Cosmochim. Acta* **72**, 2805–2821.
- Fike D. A. and Grotzinger J. P. (2008) A paired sulfate-pyrite delta S-34 approach to understanding the evolution of the Ediacaran–Cambrian sulfur cycle. *Geochim. Cosmochim. Acta* **72**(11), 2636–2648.
- Fisher I. S. J. (1986) Pyrite formation in bioturbated clays from the Jurassic of Britain. *Geochim. Cosmochim. Acta* **50**, 517–523.
- Fisher I. S. J. and Hudson J. D. (1987) Pyrite formation in Jurassic shales of contrasting biofacies. In *Marine Petroleum Source Rocks*, vol. 26 (eds. J. Brooks and A. J. Fleet). Geological Society of London Special Publication, London, pp. 69–78.
- Fry B., Gest H. and Hayes J. M. (1984) Isotope effects associated with the anaerobic oxidation of sulfide by the purple photosynthetic bacterium, *Chromatium-Vinosum*. *FEMS Microbiol. Lett.* **22**(3), 283–287.
- Fry B., Ruf W., Gest H. and Hayes J. M. (1988) Sulfur isotope effects associated with oxidation of sulfide by O-2 in aqueous solution. *Chem. Geol.* **73**(3), 205–210.
- Gaffin S. (1987) Ridge volume dependence on seafloor generation rate and inversion using long-term sealevel change. *Am. J. Sci.* **287**, 596–611.
- Garrels R. M. and Lerman A. (1981) Phanerozoic cycles of sedimentary carbon and sulfur. *Proc. Natl. Acad. Sci. USA* **78**, 4550–4656.
- Garrels R. M. and Lerman A. (1984) Coupling of sedimentary sulfur and carbon cycles – an improved model. *Am. J. Sci.* **284**, 989–1007.
- Gautier D. L. (1985) Sulfur/carbon ratios and sulfur isotope composition of some cretaceous shale from the western interior of North America, U.S. Geological Survey.
- Gautier D. L. (1985) Sulfur/carbon ratios and sulfur isotope composition of some cretaceous shale from the western interior of North America, U.S. Geological Survey.
- Geldsetzer H. J., Goodfellow W. D., Mc Laren D. J. and Orchard M. J. (1987) Sulfur-isotope anomaly associated with the Frasnian–Famennian extinction, Medicine lake, Alberta, Canada. *Geology* **15**, 393–396.
- Gorjan P., Veevers J. J. and Walter M. R. (2000) Neoproterozoic sulfur-isotope variation in Australia and global implications. *Precambrian Res.* **100**, 151–179.
- Haq B. U. and Schutter S. R. (2008) A chronology of Paleozoic sea-level changes. *Science* **322**, 64–68.
- Hattori K., Campbell F. A. and Krouse H. R. (1983) Sulphur isotope abundance in Aphebian clastic rocks: implications for the coeval atmosphere. *Nature* **302**, 323–326.
- Holser W. T., Schidlowski M., Machenzie F. T. and Maynard J. B. (1988) *Chemical Cycles in the Evolution of Earth*. Wiley Press, New York.
- Hurtgen M. T., Halverson G. P., Arthur M. A. and Hoffman P. F. (2006) Sulfur cycling in the aftermath of a 635-Ma snowball glaciation: evidence for a syn-glacial sulfidic deep ocean. *Earth Planet. Sci. Lett.* **245**(3–4), 551–570.
- Johnston D. T., Wing B. A., Farquhar J., Kaufman A. J., Strauss H., Lyons T. W., Kah L. C. and Canfield D. E. (2005a) Active microbial sulfur disproportionation in the Mesoproterozoic. *Science* **310**, 1477–1479.
- Johnston D. T., Farquhar J., Wing B. A., Kaufman A., Canfield D. E. and Habicht K. S. (2005b) Multiple sulfur isotope fractionations in biological systems: a case study with sulfate reducers and sulfur disproportionators. *Am. J. Sci.* **305**, 645–660.
- Johnston D. T., Poulton S. W., Fralick P. W., Wing B. A., Canfield D. E. and Farquhar J. (2006) Evolution of the oceanic sulfur cycle at the end of the Paleoproterozoic. *Geochim. Cosmochim. Acta* **70**, 5723–5739.
- Johnston D. T., Farquhar J. and Canfield D. E. (2007) Sulfur isotope insights into microbial sulfate reduction: when microbes meet models. *Geochim. Cosmochim. Acta* **71**, 3929–3947.
- Johnston D. T., Farquhar J., Summons R., Shen Y., Kaufman A. J., Masterson A. L. and Canfield D. E. (2008) Late Paleoproterozoic sulfur isotope biogeochemistry: insight from the McArthur Basin. *Geochim. Cosmochim. Acta* **72**, 4278–4290.
- Johnston D. T., Farquhar J., Habicht K. S. and Canfield D. E. (2008) Sulphur isotopes and the search for life: strategies for identifying sulphur metabolisms in the rock record and beyond. *Geobiology* **6**, 425–435.
- Jørgensen B. B. (1982) Mineralisation of organic matter in the sea bed – the role of sulphate reduction. *Nature* **296**, 643–645.
- Jowett E. C., Roth T., Rydzewski A. and Oszczepalski S. (1991) “Background” 34S values of Kupferschiefer sulphides in Poland: pyrite–marcasite nodules. *Miner. Deposita* **26**, 89–98.
- Kajiwara Y. and Kaiho K. (1992) Oceanic anoxia at the Cretaceous/Tertiary boundary supported by the sulfur isotopic record. *Palaeogeogr. Palaeoclimatol. Paleocool* **99**, 151–162.
- Kampschulte A. and Strauss H. (2004) The sulfur isotopic evolution of Phanerozoic seawater based on the analysis of structurally substituted sulfate in carbonates. *Chem. Geol.* **204**, 255–286.
- Kampschulte A., Bruckschen P. and Strauss H. (2001) The sulphur isotopic composition of trace sulphates in Carboniferous brachiopods: implications for coeval seawater, correlation with other geochemical cycles and isotope stratigraphy. *Chem. Geol.* **175**, 149–173.
- Knoll A. H. (1992) Biological and biogeochemical preludes to the Ediacaran radiation. In *Origin and Early Evolution of the Metazoa* (eds. J. H. Lipps and P. W. Signor). Plenum Press, New York, pp. 53–84.
- Korte C. (1999) ⁸⁷Sr/⁸⁶Sr, d¹⁸O- und d¹³C-Evolution des triassischen Meerwassers: Geochemische und stratigraphische Untersuchungen an Conodonten und Brachiopoden. *Bochum. Geol. Geotechn. Arb.* **52**, 171S.
- Kurtz A. C., Kump L. R., Arthur M. A., Zachos J. C. and Paytan A. (2003) Early Cenozoic decoupling of the global carbon and sulfur cycles. *Paleoceanography* **18**. doi:10.1029/2003PA000908.

- Logan G. A., Calver C. R., Gorjan P., Summons R. E., Hayes J. M. and Walter M. R. (1999) Terminal proterozoic mid-shelf benthic microbial mats in the centralian superbasin and their environmental significance. *Geochim. Cosmochim. Acta* **63**, 1345–1358.
- Lowenstein T. K., Hardie L. A., Timofeeff M. N. and Demicco R. V. (2003) Secular variation in seawater chemistry and the origin of calcium chloride basinal brines. *Geology* **31**, 857–860.
- Marowsky G. (1969) Schwefel-, Kohlenstoff- und Sauerstoff-Isotenenuntersuchungen am Kupferschiefer als Beitrag zur genetischen Deutung. *Contr. Mineral. Petrol.* **22**, 290–334.
- Murowchick J. B., Coveney R. M., Grauch R. I., Eldridge C. S. and Shelton K. L. (1994) Cyclic variations of sulfur isotopes in Cambrian stratabound Ni–Mo–(Pge–Au) ores of Southern China. *Geochim. Cosmochim. Acta* **58**(7), 1813–1823.
- Ono S., Wing B. A., Johnston D. T., Farquhar J. and Rumble D. (2006) Mass-dependent fractionation of quadruple stable sulfur isotope system as a new tracer of sulfur biogeochemical cycles. *Geochim. Cosmochim. Acta* **70**, 2238–2252.
- Prokoph A., Shields G. A. and Veizer J. (2008) Compilation and time-series analysis of a marine carbonate delta O-18, delta C-13, Sr-87/Sr-86 and delta S-34 database through Earth history. *Earth Sci. Rev.* **87**(3–4), 113–133.
- Railsbeck L. B. (1989) *Ordovician paleoceanography: stable isotope and C–S–Fe evidence from the Caradocian Trenton Group, Mohawk Valley*. University Illinois, Urbana-Champaign, New York.
- Raiswell R., Bottrell S. H., Al-Biatty H. J. and Tan M. M. D. (1993) The influence of bottom water oxygenation and reactive iron content on sulfur incorporation into bitumens from Jurassic marine shales. *Am. J. Sci.* **293**, 569–596.
- Rickard D. T., Zweifel H. and Donnelly T. H. (1979) Sulfur isotope systematics in the Åsen pyrite–barite deposits, Skellefte District, Sweden. *Econ. Geol.* **74**, 1060–1068.
- Ripley E. M. and Nicol D. L. (1981) Sulfur isotopic studies of Archean slate and graywacke from northern Minnesota: evidence for the existence of sulfate reducing bacteria. *Geochim. Cosmochim. Acta* **45**, 839–846.
- Ross G. M., Bloch J. D. and Krouse H. R. (1995) Neoproterozoic strata of the Southern Canadian Cordillera and the isotopic evolution of seawater sulfate. *Precambrian Res.* **73**(1–4), 71–99.
- Rouxel O., Ono S., Alt J., Rumble D. and Ludden J. (2008) Sulfur isotope evidence for microbial sulfate reduction in altered oceanic basalts at ODP site 801. *Earth Planet. Sci. Lett.* **268**, 110–123.
- Schmitz B., Andersson P. and Dahl J. (1988) Iridium, sulfur isotopes and rare earth elements in the Cretaceous-Tertiary boundary clay at Stevns Klint, Denmark. *Geochim. Cosmochim. Acta* **52**, 229–236.
- Strauss H. (1999) Geological evolution from isotope proxy signals – sulfur. *Chem. Geol.* **161**, 89–101.
- Strauss H., Bengtson S., Myrow P. M. and Vidal G. (1992) Stable isotope geochemistry and palynology of the late Precambrian to Early Cambrian sequence in Newfoundland. *Can. J. Earth Sci.* **29**, 1662–1673.
- Thode H. G., Monster L. and Dunford H. B. (1961) Sulphur isotope geochemistry. *Geochim. Cosmochim. Acta* **25**, 159–174.
- Underwood C. J. and Bottrell S. H. (1994) Diagenetic controls on multiphase pyritization of graptolites. *Geol. Mag.* **131**, 315–327.
- Werne J. P., Hollander D. J., Lyons T. W. and Sinningh Damste J. S. (2004) Organic sulfur biogeochemistry: recent advances and future research directions. *Geol. Soc. Am. Spec. Pap.* **379**, 135–150.
- Whittaker S. G. and Kyser T. K. (1990) Effects of sources and diagenesis on the chemical composition of carbon and sulfur in Cretaceous shales. *Geochim. Cosmochim. Acta* **54**, 2799–2810.
- Zaback D. A. and Pratt L. M. (1992) Isotopic composition and speciation of sulfur in the Miocene Monterey formation: reevaluation of sulfur reactions during early diagenesis in marine environments. *Geochim. Cosmochim. Acta* **56**, 763–774.
- Zerkle A. L., Farquhar J., Johnston D. T., Cox R. P. and Canfield D. E. (2009) Fractionation of multiple sulfur isotopes during phototrophic oxidation of sulfide and elemental sulfur by a green sulfur bacterium. *Geochim. Cosmochim. Acta* **73**, 291–306.

Associate editor: David Cole